Journal of Nonlinear Mathematical Physics Volume 14, Number 2 (2007), 188–229 Article

A multidimensional superposition principle: numerical simulation and analysis of soliton invariant manifolds I

Alexander A ALEXEYEV

Department of Mathematics 1, Faculty of Cybernetics, Moscow State Institute of Radio Engineering, Electronics and Automatics, 78 Vernadskogo Avenue, Moscow 117454, Russian Federation
Laboratory of Computer Physics and Mathematical Simulation, Research Division, Room 247, Faculty of Phys.-Math. & Natural Sciences, Peoples' Friendship University of Russia, 6 Miklukho-Maklaya Street, Moscow 117198, Russian Federation
E-mail: aalexeyev@mtu-net.ru

Received October 21, 2005; Accepted in Revised Form December 22, 2006

Abstract

In the framework of a multidimensional superposition principle involving an analytical approach to nonlinear PDEs, a numerical technique for the analysis of soliton invariant manifolds is developed. This experimental methodology is based on the use of computer simulation data of soliton–perturbation interactions in a system under investigation, and it allows the determination of the dimensionality of similar manifolds and partially (in the small amplitude perturbation limit) to restore the related superposition formulae. Its application for cases of infinite dimensionality, and the question of approximation by lower dimensional manifolds and, respectively, by superposition formulae of a lower order are considered as well. The ideas and implementation details are illustrated and verified by using examples with the integrable, MKdV and KdV equations, and also nonintegrable, Kawahara and Regularized Long Waves equation, soliton models.

1 Introduction

A Multidimensional Superposition Principle [3, 4, 6] was proposed as an approach for obtaining *Superposition Formulae* of solutions of nonlinear PDEs, which for solitonic equations are general solutions describing an interaction of a soliton with another wave. In the framework of this method the most critical moment is finding invariant manifolds leading to such formulae. A direct technique for this in the case of *Invariant Manifolds of the Soliton type* [4] involves solving a system of determining equations, that requires considerable computer resources and time. Naturally, the following question arises: Whether one could use a numerical simulation either for finding IMSs and SFs, or at least for the verification of their existence and for determining their parameters, because the cost of a

numerical experiment and all the accompanying requirements of computer resources are incomparably lower than those involved when using symbolic computations?

The present work is devoted to the development of such a methodology for the experimental (from data of soliton interaction numerical modelling) investigation of IMSs. Two experimental schemes are considered. One of them is based on studying local deformations of a soliton, while another takes into consideration a soliton envelope in the whole. The first technique allows us to observe and control excitation of soliton parameters in every point of the space, that may be important for some tasks and applications (e.g., in the theory of elasticity or particles physics, where they can be associated with internal degrees of freedom), and respectively determine IMS dimensionality for finite dimensional cases. In the last cases (presumably these are so-called integrable equations) a priori knowledge of this dimensionality allows us to get rid of useless and highly wasteful computational work when finding analytical expressions for the IMSs, because the direct technique supposes consequent consideration of the above-mentioned determining equations for each concrete dimensionality. However, this technique does not give the exact quantitative characteristics of the modulation. In this connection the next obvious question is: How to obtain such characteristics and how to work with infinitely dimensional or approximate IMSs? One more important question is whether this methodology can be used not only purely for the analysis but also for direct reconstruction of an SF for an equation under investigation. The answers to these questions can partially be obtained already using the global analysis.

The plan of the remaining part of the paper is as follows: In Section 2 the definitions associated with the MSP are given, and some indications of its applications are given. The technique of local analysis is presented in Section 3, where firstly the theoretical background is given in Section 3.1, and the scheme for computer simulation is given in Section 3.2, and then the approach is demonstrated in the experiments with the soliton solutions of the well-known MKdV and KdV equations, which are two integrable equations for which the related analytical results are known. In the next section, Section 4, the technique of global analysis is developed for determining the IMSs dimensionality, with Section 4.1 and 4.2 devoted to finding SFs of solitons with low amplitude waves. As an example, the investigation of the IMS for the kink of the same MKdV equation is carried out; the above type SF is restored and then compared with the known analytical expression. The global analysis is developed further in Section 5, where the issues of approximate IMSs and SFs are addressed. Two nonintegrable models, the Kawahara and Regularized Long Wave equations, are considered as examples. Some remarks and comments about the numerical methods used and the results obtained are made in Section 6. In the same section some questions important for the practical application of the technique are elucidated. Finally, a conclusion is given in the last section.

2 The main definitions of the multidimensional superposition principle

Here, we will recall the main definitions and ideas of the MSP.

Definition [3, 4]. Let there to be some PDE in the simplest case of the form

$$\frac{\partial}{\partial t}u = E\left(\frac{\partial}{\partial x}; u\right), \qquad u = u(x,t) \tag{2.1}$$

and another PDE

$$\frac{\partial}{\partial t}u = E\left(\frac{\partial}{\partial x_1} + \frac{\partial}{\partial x_2}; u\right), \qquad u = u(x_1, x_2, t) \tag{2.2}$$

obtained from the former by the formal change of the differential operator $\frac{\partial}{\partial x} = \frac{\partial}{\partial x_1} + \frac{\partial}{\partial x_2}$, so that solutions $u(x,t)$ for (2.1) are the projections of solutions $u(x_1, x_2, t)$ for (2.2)

$$u(x,t) = u(x_1, x_2, t)|_{x_1 = x_2 = x} \tag{2.3}$$

(we will call equation (2.2) *the d-adjoint* to (2.1)). If this last equation has an invariant manifold [20] being described by differential relations of the following forms

$$Q\left(u, u_{x_1}, \ldots, u_{nx_1}\right) = 0, \qquad n \in \mathbb{N} \tag{2.4}$$

and respectively

$$G_j\left(\frac{\partial}{\partial x_2}; u, u_{x_1}, \ldots, u_{(n-1)x_1}\right) = 0, \qquad j = 1, \ldots, n';\ n' \in \mathbb{N} \tag{2.5}$$

on the strength of the elimination of terms with $\frac{\partial}{\partial t}$ and $\frac{\partial^n}{\partial x^n}$ in view of (2.2) and (2.4), then equation (2.4) will be called *a soliton envelope equation*, equations (2.5) are *linkage equations*, and the above invariant manifold itself is *an invariant manifold of the soliton type*.

As a consequence, functions $u(x_1, x_2, t)$ in (2.4) and (2.5) will have the structure

$$u(x_1, x_2, t) = F\Big(x_1; \theta_1(x_2, t), \ldots, \theta_n(x_2, t)\Big), \tag{2.6}$$

with the form of F is determined by the ODE (2.4), while the remaining equations, equations (2.5), determine the linkages between the θ_j. In doing so, the solution $u(x,t)$ in (2.3) can be interpreted as a soliton with the parameters θ_j modulated by some perturbation and respectively describes their mutual superposition.

Note 1. In the cases with *static solitons*, i.e. when a soliton is possibly moving with some speed but does not change its form, θ_j can be recalibrated so as to explicitly display the obvious combination $x - v_s t$ in (2.6), see the examples in [4].

On the level of the invariant manifolds, the MSP at least intersects with, if not advances, the Lie-symmetry analysis [4]. And in contrast to many other approaches, it allows one to solve a problem 'in reverse' and find equations admitting solutions with soliton properties rather then solutions of a known soliton equation, [4] again. Such a task is characteristic of reaction–diffusion models, where general structure is fixed, while the nonlinearity and source belong to some classes. In some cases it is necessary to distinguish equations

possessing soliton solutions knowing nothing of their form. Up to date, using classical analysis, it was possible only to indicate models with localized waves without diagnostication of their properties (see, e.g., [31], Section 5.5.2, [29] and references therein).

At the same time, on the level of superposition formulae (2.6), the MSP is in essence the generalization of the well-known collective-variable approach (see, e.g., [30] for references), and similar problems on weak modulation of solitons are traditional for nonlinear physics. The soliton variable x_1 and the variable x_2 associated with a perturbation here play a role of the fast and slow variables. The central point of this method involves choosing the form of an envelope and its parameters that are being modulated. While there exists no theory for this in the framework of this method itself, an unperturbed soliton profile with a suitable number of obvious physical parameters like a wave number and an amplitude are used usually, this can effectively be solved in the MSP.

In principle, the superposition formulaes can be used for constructing new solutions from known ones. Obviously, however, that direct derivation is limited to more or less simple expressions or equations, which for well-studied models could frequently be obtained via other techniques. The idea to obtain from the MSP a rigorous theory of the Hirota substitutions and their generalization to nonintegrable cases seems to be very attractive (in this connection we mention the works [19, 13, 7] and [26, 27]) but this demands a deeper understanding of the structures of soliton invariant manifolds.

At present, the most essential impact of the superposition formulas is a transparent description of the interaction mechanism. Up to now, it has not received proper attention in the soliton science. Partially, on the one hand, such situation are explained by simple enough dynamics in so-called integrable systems, the main object of the study, and the absence of a general approach for other equations on the other hand. However, integrable models are very rare among physical models. Moreover, the purposeful use of solitons in and for various applications leads us to the other types of problem. First of all, this is the description of various secondary effects arising under interactions of solitonic structures with other waves. The dominant effect for most known solitonic equations, both integrable and nonintegrable ones, is reduced to a phase shift. But secondary effects frequently result in consequences more serious from the physical viewpoint, e.g., generation of parasitic radiation, formation of boundary states, etc. One more issue is interactions of weak, linear, waves with solitons. From a technical standpoint, these may be both the usual noise and pumping impulses or continuous waves. Last but not least, a very perspective direction for further development of the soliton science is the use of soliton interactions for technological applications such as information processing and computer CPUs. — One will note respectively [22, 1, 25] as the review works for the subjects touched upon here and [24] together with the related references therein as one perturbation theory for similar problems.

The common feature of all the above issues is that they deal with either low amplitude waves or asymptotical properties, say, the influence of a tail of one soliton on another. In these cases various linearizations or limit cases of the related SFs can be effectively used either for a full description of interactions in the former case or for a description of asymptotical states of solitons in the latter one. The very general point was expressed in [3]. As was shown there, both switching solitons from one state to another and the inelastic effects of interactions can be associated with the properties of θ. In the simplest statement the problem is reduced to an investigation of the asymptotic form $\theta(x,t) \to \text{const} + \text{o}(1)$

in SFs like, e.g., (3.9). In the more general statement the analysis can be performed purely numerically in view of the ODE nature of degenerations of superposition formulas corresponding to asymptotical states of a perturbation (see (3.11) below as such an example). In this connection in [5] a number of the computer experiments are fulfilled with the purpose of comparing solitonic interactions in integrable and nonintegrable models in respect of the properties peculiar to the above SFs. The main feature of them is that they used a technique that allows one to avoid distortion of the picture by most of inelastic effects describable in the framework of the MSP. The results obtained indicate that the superposition is of universal character, and the derivations from the ideal picture is small enough and could, in principle, be explained by the natural limitations of the computer simulation.

3 The local analysis of soliton deformation and IMS dimensionality

3.1 The theoretical background

Our goal now is to indicate a way for determining the order of equation (2.4), i.e. *the dimensionality of an IMS, knowing only the original equation* (2.2). For this purpose consider some solution u_0 of equation (2.2) together with other equations u_i close to the first one

$$u_i(x_1, x_2, t) = u_0(x_1, x_2, t) + \delta v_i(x_1, x_2, t), \qquad |\delta| \ll 1. \tag{3.1}$$

Linearization of (2.4) for v_i on the background of u_0 gives us

$$\delta\Big(Q_u|_{u=u_0} v_i + Q_{u_{x_1}}\big|_{u=u_0} v_{i,x_1} + \cdots + Q_{u_{nx_1}}\big|_{u=u_0} v_{i,nx_1} \Big) = \mathrm{O}(\delta^2). \tag{3.2}$$

The order of the linearized ODE to v_i identical to the dimensionality sought equals to the maximal number of its linearly independent solutions. The following proposition takes place as a direct consequence of the well-known theorem on a Wronskian, see e.g. [15].

Proposition 1. The number of linearly independent functions in $\{y_1(x), \ldots, y_m(x)\}$ is equal to a rank of the matrix

$$\hat{W}[\vec{y}] = \begin{pmatrix} y_1 & y_2 & \cdots & y_m \\ y_1^{(1)} & y_2^{(1)} & \cdots & y_m^{(1)} \\ \cdots & \cdots & \cdots & \cdots \\ y_1^{(l)} & y_2^{(l)} & \cdots & y_m^{(l)} \end{pmatrix}, \qquad l \geq m.$$

In other words, for the matrix

$$\hat{W}[\delta\vec{v}] = \begin{pmatrix} \delta v_1 & \delta v_2 & \ldots & \delta v_m \\ \delta v_{1,x_1} & \delta v_{2,x_1} & \ldots & \delta v_{m,x_1} \\ \cdots & \cdots & \cdots & \cdots \\ \delta v_{1,lx_1} & \delta v_{2,lx_1} & \ldots & \delta v_{m,lx_1} \end{pmatrix}, \qquad l, m \geq n \tag{3.3}$$

in all points (x_1, x_2, t) we have

$$\lim_{\delta \to 0} \max_{\text{all sets } \{v_1,\ldots,v_m\}} \text{rank } \hat{W}[\delta \vec{v}] \leq n.$$

Where the sign '$<$' in particular takes into account the circumstance that in some points not all solution parameters may be modulated or modulated adequately.

We now offer some comments on the implementation aspects of this approach.

The best way for finding the rank of some matrix, say $\hat{M}$ of $m_1 \times m_2$, is to use its *Singular Values Decomposition*

$$\hat{M}_{ij} = \sum_{l=1}^{m} \hat{U}_{il} s_l \hat{V}_{jl}, \qquad m = \min\{m_1, m_2\}, \tag{3.4}$$

see [28] as a good introduction. Here $\hat{U}$ and $\hat{V}$ are matrixes, $m_1 \times m_2$ and $m_1 \times m_1$ respectively, with the orthonormal columns

$$\sum_j \hat{U}_{jl_1} \hat{U}_{jl_1} = \delta_{l_1 l_2}, \ \sum_j \hat{V}_{jl_1} \hat{V}_{jl_1} = \delta_{l_1 l_2} \tag{3.5}$$

and s_l, the so-called singular numbers, are ordered in the following manner

$$s_1 \geq s_2 \geq \cdots \geq s_m.$$

The number of nonzero singular numbers is equal to the rank (in the framework of a simulation accuracy, certainly). Next, obviously, instead of 'all sets' of v_i their *finite number generated from random initial data* can be taken.

Further an experimental technique based on these facts is presented in detail.

3.2 The scheme of an experiment. The examples with the MKdV and KdV soliton solutions

Although the values of u_{i,jx_1} needed for $\hat{W}[\delta \vec{v}]$ (3.3) cannot be calculated directly from $u_i(x,t)$, but for points (x,x,t) they can be obtained together with u_i numerically.

Really, since their evolutions are described by the obvious consequences of (2.2)

$$\frac{\partial}{\partial t}\left(u_{i,jx_1}\right) = \frac{\partial^j}{\partial x_1^j} E\left(\frac{\partial}{\partial x_1} + \frac{\partial}{\partial x_2}; u_i\right), \qquad u_i = u_i(x_1, x_2, t)$$

then to find their magnitudes it is enough to solve a system of the form

$$\begin{aligned}
&\tilde{u}_{0,t} = E\left[\frac{\partial}{\partial x}; \tilde{u}_0\right], \quad \tilde{u}_0 = \tilde{u}_0(x,t) \\
&\tilde{u}_{1,t} = E_1\left[\frac{\partial}{\partial x}; \tilde{u}_0, \tilde{u}_1\right], \quad \tilde{u}_1 = \tilde{u}_1(x,t) \\
&\cdots \\
&\tilde{u}_{l,t} = E_l\left[\frac{\partial}{\partial x}; \tilde{u}_0, \tilde{u}_1, \ldots, \tilde{u}_l\right], \quad \tilde{u}_l = \tilde{u}_l(x,t)
\end{aligned} \tag{3.6}$$

(here $\tilde{u}_j(x,t) \equiv u_{jx_1}(x_1,x_2,t)|_{x_1=x_2=x}$, and the index of an experiment has been omitted) with the related initial data

$$\tilde{u}_0(x,0) = \psi_0(x) \equiv \psi(x_1,x_2)|_{x_1=x_2=x}$$
$$\dots$$
$$\tilde{u}_l(x,0) = \psi_l(x) \equiv \psi_{lx_1}(x_1,x_2)|_{x_1=x_2=x}$$

and suitable boundary conditions (usually $\tilde{u}_0(\pm\infty,t) = \text{const}$ and $\tilde{u}_j(\pm\infty,t) = 0$ for $j > 0$).

The next question is how to construct the necessary initial data, i.e. $\psi_j(x)$, for each of the experiments. If one assumes that at an initial moment a soliton and a perturbation are not overlapping, it is trivial

$$\psi_0(x) = \Big(u_{\text{soliton}}(x_1) + u_{\text{perturbation}}(x_2)\Big)\Big|_{x_1=x_2=x} = u_{\text{soliton}}(x) + u_{\text{perturbation}}(x)$$

and, as a consequence

$$\psi_j(x) = u^{(j)}_{\text{soliton}}(x), \quad j > 0.$$

According to (3.3) and (3.1) it is necessary to have the results of several experiments with close $\vec{\tilde{u}}_i = (\tilde{u}_0,\dots,\tilde{u}_l)_i$ and respectively close initial data. From the technical viewpoint the simplest way to realize this is to add to a localized perturbation chosen (we will call this common for all experiments part *a carrier*) an analogously localized and *randomly generated noise*, so that for each case

$$u_{\text{perturbation}_i}(x) = u_{\text{carrier}}(x) + \delta u_{\text{noise}\,i}(x).$$

Also, it is convenient to have one experiment without such noise for $\vec{\tilde{u}}_0$. By this means the expression for the elements of $\hat{W}[\delta\vec{v}]$ is as follows

$$\hat{W}_{ij} = \tilde{u}_{j+1,i} - \tilde{u}_{j+1,0}.$$

Here the first subscript is associated with the order of the derivative, and the second is with the number of an experiment. The rank of $\hat{W}[\delta\vec{v}]$ is equal to the quantity of soliton parameters being modulated by a perturbation. It is maximal in an interaction zone and minimal (the unit) out of it, or if an interaction is absent.

Further the methodology being proposed is illustrated by its application for determining the dimensionalities of the IMSs associated with the solitons of the MKdV (both the kink and bell-shape solution) and KdV equations. The accuracy in the experiments was $\varepsilon \sim 10^{-13}, 10^{-16}$ at $\delta = 10^{-5}, 5\cdot 10^{-8}$ respectively for $u_{\text{noise}}(x)$ normalized to the unit, i.e. $\max|u_{\text{noise}}(x)| = 1$. This relation, $\varepsilon \sim \delta^2$, turns out to be optimal from the practical viewpoint when taking into account the structure of (3.2). In order to achieve such an accuracy, the spectral (Fourier expansion) technique [9] was applied on the spatial variable together with the Runge-Kutta exponential time differencing method of the fourth order [11] for time integration of coefficients in these expansions. The former implies periodical boundary conditions natural in the case with bell-shape solitons but demanding some specific carriers for experiments with the kink solutions. In all points of the space the singular numbers s_l of $\hat{W}[\delta\vec{v}]$ were calculated, and in all the figures with plots of s_l, $\log s_l$

versus x, the singular numbers are normalized in such manner that $s_1 = 1$. After the collapse of an initial disturbance $s_1 \sim \delta$ everywhere, that reflects the presence of the perturbation. To be precise, s_1 will be as much as the amplitude of a steady-state noise in a system, where the last one also depends essentially on L. In particular, because of this the use of $\hat{W}[\delta\vec{v}]$ rather than $\hat{W}[\vec{v}]$ is more convenient. The normalization makes the picture clearer and robust smoothing fluctuations from the changing amplitude of a perturbation, while the non-normalized values of s_1 can, in principle, be used for its estimation.

Example 1 (modulation of the MKdV kink). In [4] it was shown that the adjoint equation to the MKdV

$$u_t - 6u^2u_x + u_{xxx} = 0, \qquad u = u(x,t) \tag{3.7}$$

has the following IMS

$$\begin{aligned} &2u_{x_1x_1x_1}u_{x_1} - 3u_{x_1x_1}^2 + k_{\rm s}^2u_{x_1}^2 = 0, \qquad u = u(x_1,x_2,t),\ k_{\rm s} = \text{const} \\ &u_{x_1x_1} + u_{x_1x_2} \mp 2uu_{x_1} = 0 \\ &2u_{x_1}u_{x_1x_1x_2} + 3u_{x_1x_1}^2 - k_{\rm s}^2u_{x_1}^2 \mp 4u_{x_1}\left(u_{x_1}^2 + uu_{x_1x_1}\right) = 0. \end{aligned} \tag{3.8}$$

The related SF after the projection (2.3) gives

$$\begin{aligned} u(x,t) = \pm\left[\left(\frac{k_{\rm s}+\theta_x}{2}\right)\tanh\left(\frac{k_{\rm s}x + \frac{k_{\rm s}^3}{2}t + \theta}{2}\right) - \frac{\theta_{xx}}{2\left(k_{\rm s}+\theta_x\right)}\right], \\ k_{\rm s} = \text{const},\ \theta = \theta(x,t) \end{aligned} \tag{3.9}$$

corresponding to the superposition of the MKdV kink

$$u_{\rm kink/anti-kink}(x,t) = \pm\frac{k_{\rm s}}{2}\tanh\left(\frac{k_{\rm s}x + \frac{k_{\rm s}^3}{2}t + \varphi}{2}\right), \qquad k_{\rm s},\varphi = \text{const} \tag{3.10}$$

with an arbitrary perturbation associated with the function θ (φ is included into θ). In doing so, θ itself satisfies the equation

$$2\theta_t + 2\theta_{xxx} - \theta_x^3 - 3k_{\rm s}\theta_x^2 - 3k_{\rm s}^2\theta_x - \frac{3\theta_{xx}^2}{\theta_x + k_{\rm s}} = 0, \quad \theta = \theta(x,t)$$

such that the limit cases of (3.9) at $k_{\rm s}x + \frac{k_{\rm s}^3}{2}t \to \pm\infty$, namely

$$\begin{aligned} u_{\text{perturbation}_{+\infty}} &= \pm\left[\left(\frac{k_{\rm s}+\theta_x}{2}\right) - \frac{\theta_{xx}}{2\left(k_{\rm s}+\theta_x\right)}\right] \\ u_{\text{perturbation}_{-\infty}} &= \pm\left[-\left(\frac{k_{\rm s}+\theta_x}{2}\right) - \frac{\theta_{xx}}{2\left(k_{\rm s}+\theta_x\right)}\right] \end{aligned} \tag{3.11}$$

again satisfy (3.7). Moreover, in particular for θ with the asymptotes

$$\lim_{x\to\pm\infty}\theta(x,t) = \theta_\pm = \text{const}$$

it will be the localized perturbation, and the expressions (3.11) will describe its states before and after the interaction with the kink (respectively, the difference $\theta_- - \theta_+$ determines the phase shift of the latter).

For the above simulation the following system (3.6) was used

$$\begin{aligned} &\tilde{u}_{0,t} + \lambda\tilde{u}_{0,x} - 2\left(\tilde{u}_0^3\right)_x + \tilde{u}_{0,xxx} = 0, \quad \tilde{u}_0 = \tilde{u}_0(x,t) \\ &\tilde{u}_{1,t} + \lambda\tilde{u}_{1,x} - 6\left(\tilde{u}_0^2\tilde{u}_1\right) + \tilde{u}_{1,xxx} = 0, \quad \tilde{u}_1 = \tilde{u}_1(x,t) \\ &\ldots, \quad \lambda = \text{const} \end{aligned} \tag{3.12}$$

with the periodical boundary conditions

$$\tilde{u}_j(0,t) = \tilde{u}_j(L,t), \quad j \geq 0.$$

Here we have introduced the terms $\lambda\tilde{u}_{0,x}$, $\lambda\tilde{u}_{1,x}$ and so on; λ is chosen so that the soliton itself was immovable, which simplifies carrying out the experiments. Two experimental series with both weak and strong modulation of the kink were performed.

Experimental series 1 (weak modulation of the kink (3.10), $\varepsilon \sim 10^{-13}$, $\delta = 10^{-5}$, $k_\mathrm{s} = 2$) — Figures 1(*a*)–1(*d*).

The first of the figures, Figure 1(*a*), shows the initial configuration ($\tilde{u}_0$ and $\tilde{u}_1$ only, the thick solid and dashed lines respectively) needed for the experiments. As seen, here the carrier was chosen in the form of an anti-kink (also immovable) to satisfy the periodic boundary conditions and does not itself interact with the main kink under investigation. The thin line here indicates the noise position and its form in one of the experiments.

The next figure, Figure 1(*b*), demonstrates the difference $\tilde{u}_{j,1} - \tilde{u}_{j,0}$ ($j = 0, \ldots, 3$) in the interaction zone at one of the interaction moments for the same experiment, while the profiles for $\tilde{u}_{1,i} - \tilde{u}_{1,0}$ ($i = 1, \ldots, 4$) are depicted for an example in Figure 1(*c*). The last figure, Figure 1(*d*), most clearly illustrates the approach. The plots for the singular numbers (the solid lines, the hatched one indicates the solution profile at the same moment) show how they change versus the coordinate.

The first singular number, s_1, is always excited because it is associated with the presence of the noise everywhere. The values of others two, s_2 and s_3, dramatically (by the factor about 10^7) rise in the interaction area, while the remaining ones are practically at the errors level (which for the singular numbers is as order as 10^{-7} here). This means that, as expected in view of (3.8) or (3.9), there are only three soliton parameters being modulated, and respectively the IMS dimensionality is equal to three as well.

Experimental series 2 (strong modulation of the kink, $\varepsilon \sim 10^{-13}$, $\delta = 10^{-5}$, $k_\mathrm{s} = 2$) — Figures 2(*a*)–2(*c*).

The whole the experiments are analogous to the previous series, however there is one difference. Here, to minimize accumulation of errors and various secondary effects, it is reasonable to break an experiment into two stages. The purpose of the first of them is to collide the carrier with the kink under investigation, and the second one consists of the injection of a noise into the system that is obtained. Such a two step technique appears to be justified in view of essential differences in the spreading speeds for large and small amplitude perturbations.

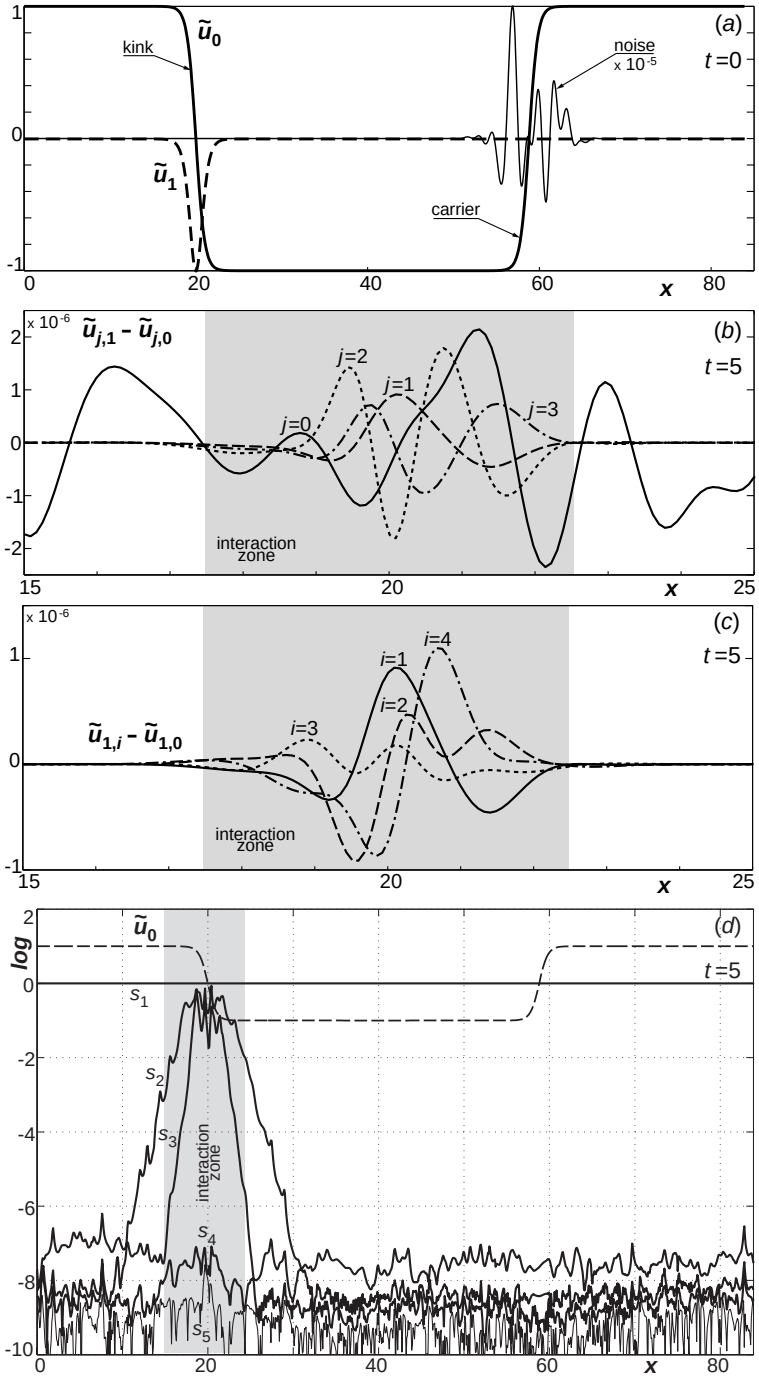

Figure 1. The local analysis, weak modulation of the MKdV kink: (a) The solid and dashed thick lines — the initial profiles of $\tilde{u}_0$ and $\tilde{u}_1$, respectively. The thin line — the noise position and form in one of the experiments. (b) The differences $\tilde{u}_{j,1} - \tilde{u}_{j,0}$ for the above experiment at one moment of the interaction. (c) The profiles of the differences $\tilde{u}_{1,i} - \tilde{u}_{1,0}$ in doing so. (d) The dependence of the singular numbers versus the coordinate (the solid lines) and the solution profile (the hatched line, schematically) at one of the moments of the interaction.

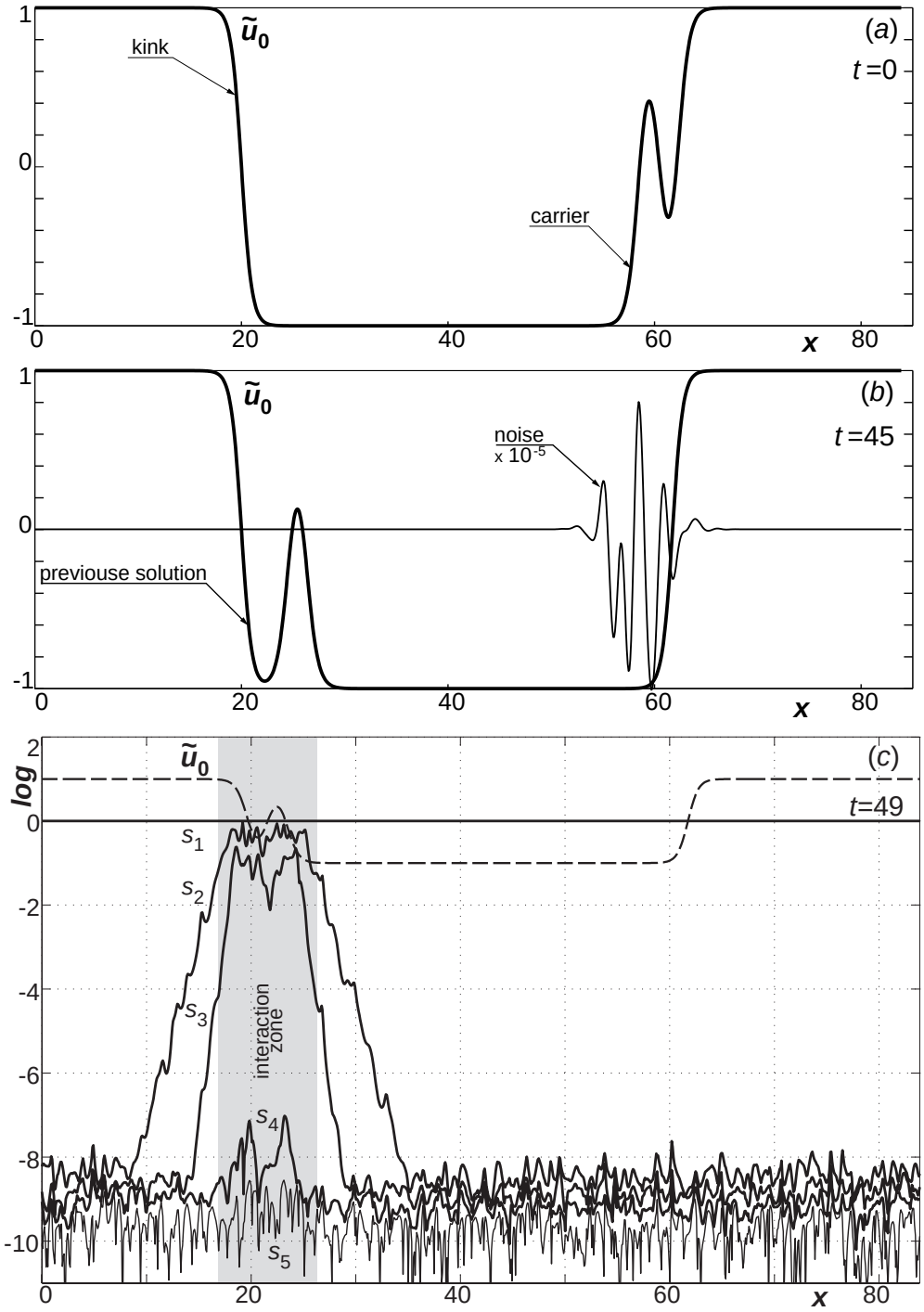

Figure 2. The local analysis, strong modulation of the MKdV kink: (*a*) The initial profile for $\tilde{u}_0$ in the first stage. (*b*) The initial profiles for $\tilde{u}_0$ in the second stage: the thick line — the initial configuration, the thin line — the noise position and typical form. (*c*) The dependence of the singular numbers versus the coordinate (the solid lines) and the solution profile (the hatched line, schematically) at the moment of the strongest kink–carrier interaction.

In Figure 2(a) the initial profile of $\tilde{u}_0$ for the first stage is shown. Here the carrier was chosen in the form of the bell-shape soliton–anti-kink configuration

$$u_{\text{carrier}}(x,t) = -\frac{k_1}{2} + \frac{\partial}{\partial x}\ln\left(\frac{1+E_1+E_2+a_{12}^2E_1E_2}{1+a_{12}E_2}\right), \quad a_{12} = \left(\frac{k_1-k_2}{k_1+k_2}\right)$$
$$E_1 = \exp\left[k_1x + \frac{k_1^3}{2}t\right],\ E_2 = \exp\left[k_2x + \left(\frac{3}{2}k_1^2k_2 - k_2^3\right)t\right], \quad k_1,k_2 = \text{const}.$$

The former will further take part in the interaction, while the latter is necessary to satisfy the boundary conditions. In the second stage the resulting profile at the suitable moment of that interaction, plus the noise, in turn is chosen as the initial data, Figure 2(b). Figure 2(c) corresponds to the moment of the strongest interaction. As in the previous case with the weak modulation, it is seen that three soliton parameters are being modulated in doing so.

Example 2 (modulation of the KdV soliton). The SF associated with the soliton of the KdV equation

$$u_t + uu_x + u_{xxx} = 0, \qquad u = u(x,t) \tag{3.13}$$

is of the form [4]

$$u(x,t) = -3\left(k_{\text{s}}+\theta_x\right)^2\tanh^2\left(\frac{k_{\text{s}}x - k_{\text{s}}^3t+\theta}{2}\right) + 6\theta_{xx}\tanh\left(\frac{k_{\text{s}}x-k_{\text{s}}^3t+\theta}{2}\right) \tag{3.14}$$
$$+\frac{3}{2}\left(k_{\text{s}}+\theta_x\right)^2 + \frac{3}{2}\left(\frac{\theta_{xx}}{k_{\text{s}}+\theta_x}\right)^2 - 3\left(\frac{\theta_{xxx}}{k_{\text{s}}+\theta_x}\right) + \frac{3}{2}k_{\text{s}}^2, \quad k_{\text{s}} = \text{const},\ \theta = \theta(x,t)$$

with the function θ in its turn satisfying the equation

$$2\theta_t + 2\theta_{xxx} - \theta_x^3 - 3k_{\text{s}}\theta_x^2 - \frac{3\theta_{xx}^2}{\theta_x+k_{\text{s}}} = 0, \quad \theta = \theta(x,t)$$

so that for the unperturbed soliton we has the familiar expression

$$u_{\text{soliton}}(x,t) = 3k_{\text{s}}^2\left[1-\tanh^2\left(\frac{k_{\text{s}}x-k_{\text{s}}^3t+\varphi}{2}\right)\right], \quad k_{\text{s}},\varphi = \text{const}. \tag{3.15}$$

As seen from (3.14), there are four parameters being modulated, and the related soliton envelope equation (2.4) will be the fourth order ODE (in [4] the explicit expressions for the IMS were obtained only for the potential version of (3.13)).

The system (3.6) for our simulation differs from one used for the MKdV (3.12) just by the obvious form of the nonlinear terms, while the periodical boundary conditions are natural here.

Experimental series 1 (weak modulation of the soliton (3.15), $\varepsilon \sim 10^{-16}$, $\delta = 5\cdot 10^{-8}$, $k_{\text{s}} = 0.5$) — Figures 3(a), 3(b).

Here, Figure 3(a), there is no need in any carrier for the boundary conditions, because the soliton asymptotes are identical. From Figure 3(b) we see that s_2, s_3 and s_4 dramatically increase from the errors level about 10^{-8} up to 10^{-2}–1 in the interaction zone.

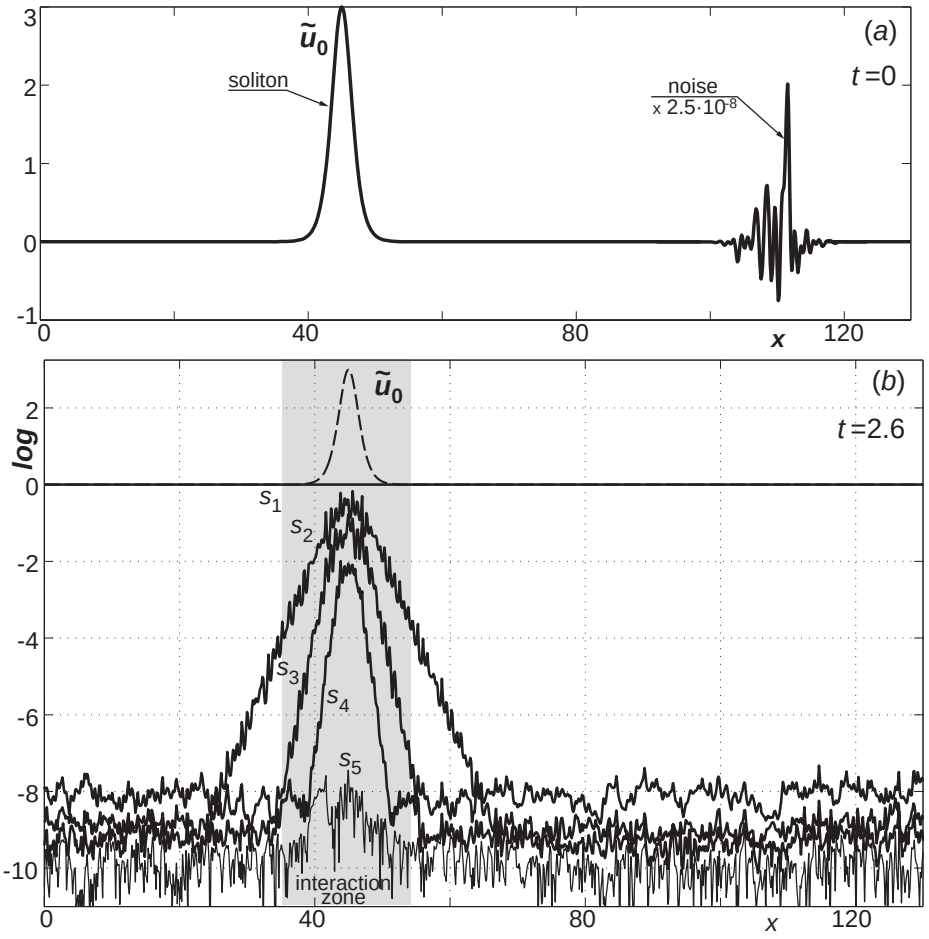

Figure 3. The local analysis, weak modulation of the KdV soliton: (*a*) The initial configuration (the noise is presented schematically). (*b*) The dependence of the singular numbers versus the coordinate (the solid lines) and the solution profile (the hatched line, schematically) at one of the moments of the interaction.

Together with s_1 this involves about four modulated parameters, and it is in agreement with the SF (3.14).

Experimental series 2 (a non-zero carrier — strong modulation of the soliton, $\varepsilon \sim 10^{-16}$, $\delta = 5 \cdot 10^{-8}$, $k_\mathrm{s} = 0.5$) — Figures 4(*a*)–4(*e*).

Figures 4(*a*), 4(*b*) are fully analogous to Figures 2(*a*), 2(*b*) and demonstrate the initial profiles of $\tilde{u}_0$ for both stages. Again, we mention (Figures 4(*c*), the moment of the strongest interaction) that four singular numbers appear in the range 10^{-2}–1, while the errors level is about 10^{-9}. Figures 4(*d*) and 4(*e*) correspond to the moments when the carrier is already far from the soliton center and basically perturbs only its tail. As expected (u_0 in the coefficients of (3.2) includes both the soliton and carrier), the singular numbers s_2, s_3 and s_4 appear to be dependent on both of them, but in such a manner that the excitation decays together with the soliton tail amplitude and disappears quite far from it.

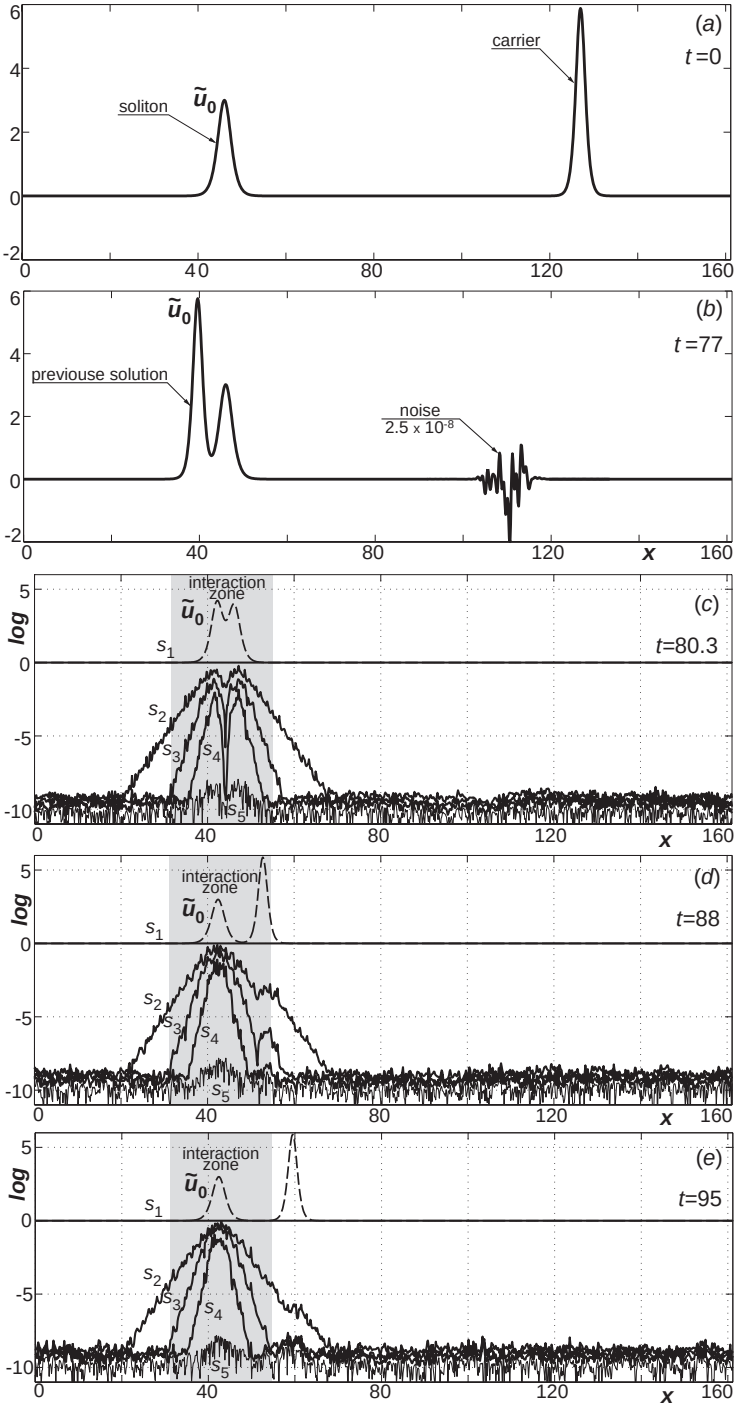

Figure 4. The local analysis, strong modulation of the KdV soliton: (*a*) The initial profile of $\tilde{u}_0$ in the first stage. (*b*) The initial profiles in the second stage with the schematically presented noise. (*c*) The dependence of the singular numbers versus the coordinate (the solid lines) and the solution profiles (the hatched line, schematically) at the moment of the strongest carrier–soliton interaction. (*d*), (*e*) The same picture at several following moments.

Example 3 (modulation of the MKdV bell-shape soliton). Although, to the best of our knowledge, neither an IMS itself associated with the MKdV bell-shape soliton nor the related SF are known yet, the latter can be easily obtained using a formalism from [3, 4, 6] based on the so-called truncated singular expansions. As was pointed out by several authors [16, 23], to construct the above soliton solution the expansions with two singular manifold functions are necessary. Applying a technique, say, from [2], we immediately have that the MKdV equation written in the form

$$u_t + 6u^2u_x + u_{xxx} = 0, \qquad u = u(x,t) \tag{3.16}$$

possesses the expansion for $u(x,t)$ of the following kind

$$u(x,t) = -i\Big[V_1(x,t) - V_2(x,t) + \theta_0(x,t)\Big]. \tag{3.17}$$

Where $V_{1,2}$ are those singular functions satisfying the system

$$\begin{aligned} &V_{j,x} = -V_j^2 - S_j/2 \\ &V_{j,t} = C_jV_j^2 - C_{j,x}V_j + (C_jS_j + C_{j,xx})/2, \quad j = 1,2,\ V_{1,2} = V_{1,2}(x,t) \end{aligned} \tag{3.18}$$

with $S_{1,2}$ and $C_{1,2}$ are subject of the compatability conditions

$$S_{j,t}+C_{j,xxx}+2S_jC_{j,x}+C_jS_{j,x} = 0, \quad j = 1,2,\ S_{1,2} = S_{1,2}(x,t),\ C_{1,2} = C_{1,2}(x,t). \tag{3.19}$$

The relations (3.18), (3.19) are common for the singular manifold approach. For (3.16) we have also to add the constraint

$$V_1V_2 = (V_1 - V_2)\theta_0 + \theta_0^2 + \gamma/6, \quad \gamma = \text{const} \tag{3.20}$$

to $V_{1,2}$, the relations between $S_{1,2}$ and $C_{1,2}$

$$C_{1,2} = S_{1,2} + \gamma, \tag{3.21}$$

and the governing equations to θ_0

$$\theta_{0,t} - 6\theta_0^2\theta_{0,x} + \theta_{0,xxx} = 0, \qquad \theta_0 = \theta_0(x,t) \tag{3.22}$$

as well as its linkage with S_1 and S_2

$$3S_{1,2} \mp 6\theta_{0,x} + 6\theta_0^2 + \gamma = 0 \tag{3.23}$$

(minus for S_1 and plus for S_2).

The expression (3.17) can be transformed to the SF sought for the bell-shape soliton with the usual asymptotes $u_{\text{bell}}(\infty,t) = 0$ if $\gamma = 3k_{\text{s}}^2/2$ and $\omega = -k_{\text{s}}^3$ taking into account the following formulae [3, 4, 6]

$$\begin{aligned} V_1 &= \left(\frac{k_{\text{s}} + \theta_x}{2}\right)\left(\frac{i\mathrm{e}^{k_{\text{s}}x+\omega t+\theta} - 1}{i\mathrm{e}^{k_{\text{s}}x+\omega t+\theta} + 1}\right) - \frac{\theta_{xx}}{2\,(k_{\text{s}} + \theta_{xx})} \\ S_1 &= -\frac{(k_{\text{s}} + \theta_x)^2}{2} - \frac{3}{2}\left(\frac{\theta_{xx}}{k_{\text{s}} + \theta_{xx}}\right)^2 + \frac{\theta_{xxx}}{k_{\text{s}} + \theta_{xx}} \\ C_1 &= -\left(\frac{\omega + \theta_t}{k_{\text{s}} + \theta_x}\right), \qquad k_{\text{s}}, \omega = \text{const};\ k_{\text{s}} \neq 0. \end{aligned} \tag{3.24}$$

The constraint (3.20) will in its turn give the expression for V_2. The final formula for the SF is obtained in a straightforward manner, but is cumbersome. Here only its structure obvious from (3.17), (3.20) and (3.24) will be important

$$u(x,t) = F\Big(k_{\rm s}x - k_{\rm s}^3 t + \theta, \theta_x, \theta_{xx}, \theta_0\Big), \tag{3.25}$$

the relation between θ_0 and θ (3.23)

$$2(\theta_x + k_{\rm s})^3\theta_x + (\theta_x + k_{\rm s})^2(4\theta_{0x} - \theta_x^2 - 4\theta_0^2) - 2(\theta_x + k_{\rm s})\theta_{xxx} + 3\theta_{xx}^2 = 0, \tag{3.26}$$

and in addition to the equation for θ_0 (3.22) the equation to θ (3.21)

$$2\theta_t + 2\theta_{xxx} - \theta_x^3 - 3k_{\rm s}\theta_x^2 - \frac{3\theta_{xx}^2}{\theta_x + k_{\rm s}} = 0, \quad \theta = \theta(x,t). \tag{3.27}$$

The solution (3.25) degenerates to the pure soliton

$$u_{\rm bell}(x,t) = k_{\rm s}\,\mathrm{sech}\left(k_{\rm s}x - k_{\rm s}^3 t + \varphi\right), \qquad k_{\rm s}, \varphi = \mathrm{const} \tag{3.28}$$

in the absence of a perturbation corresponding to the case $\theta_0 = 0, \theta = \varphi$.

The system for the simulation is identical to (3.12) with the same periodical boundary conditions, but with a positive sign in front of the nonlinear terms.

Experimental series 1 (weak modulation of the soliton (3.28), $\varepsilon \sim 10^{-16}$, $\delta = 5 \cdot 10^{-8}$, $k_{\rm s} = 1.5$) — Figures 5(a), 5(b).

Figure 5(a) gives the initial view. In Figure 5(b), as usually, we see the growth of some singular numbers from the errors level 10^{-7} up to 10^{-1}–1 in the interaction zone. Contrary to our expectations, see (3.25), the analysis shows perceptible modulation of only three parameters!

Experimental series 2 (strong modulation of the soliton, $\varepsilon \sim 10^{-16}$, $\delta = 5 \cdot 10^{-8}$, $k_{\rm s} = 1.5$) — Figures 6(a)–6(c).

Again, Figures 6(a) and 6(b) demonstrate the initial profiles of $\tilde{u}_0$ for both stages. The last one, Figure 5(c), is most interesting. As seen from it, now the singular number s_4 also increases up to the maximum about 10^{-2} in the interaction zone, i.e. all of the soliton parameters are modulated in an equal measure.

At the first glance the results obtained seem to be paradoxical, because the SF (3.25) indicates the presence of fore modulated parameters in the soliton envelope. However, a rigorous analysis shows that our experiments reflect the specific associated with the complicated linkage (3.26) between θ and θ_0. Such a specific is absent in the previous SFs, because their modulated parameters are linked with each other in a trivial manner. Here, in the general case, θ cannot be algebraically expressed in terms of θ, θ_x and θ_{xx}. But for the case of weak modulation, formally setting $|\theta|, |\theta_0| \ll 1$ (the resulting expressions are valid for any suitable θ, θ_0 corresponding to the smallness of the correction to (3.28)), we have from (3.26) and (3.22), (3.27) in the first order approximation

$$\theta_0 \simeq \left(\theta_{xx} - k_{\rm s}^2\theta\right)/(2k_{\rm s})$$

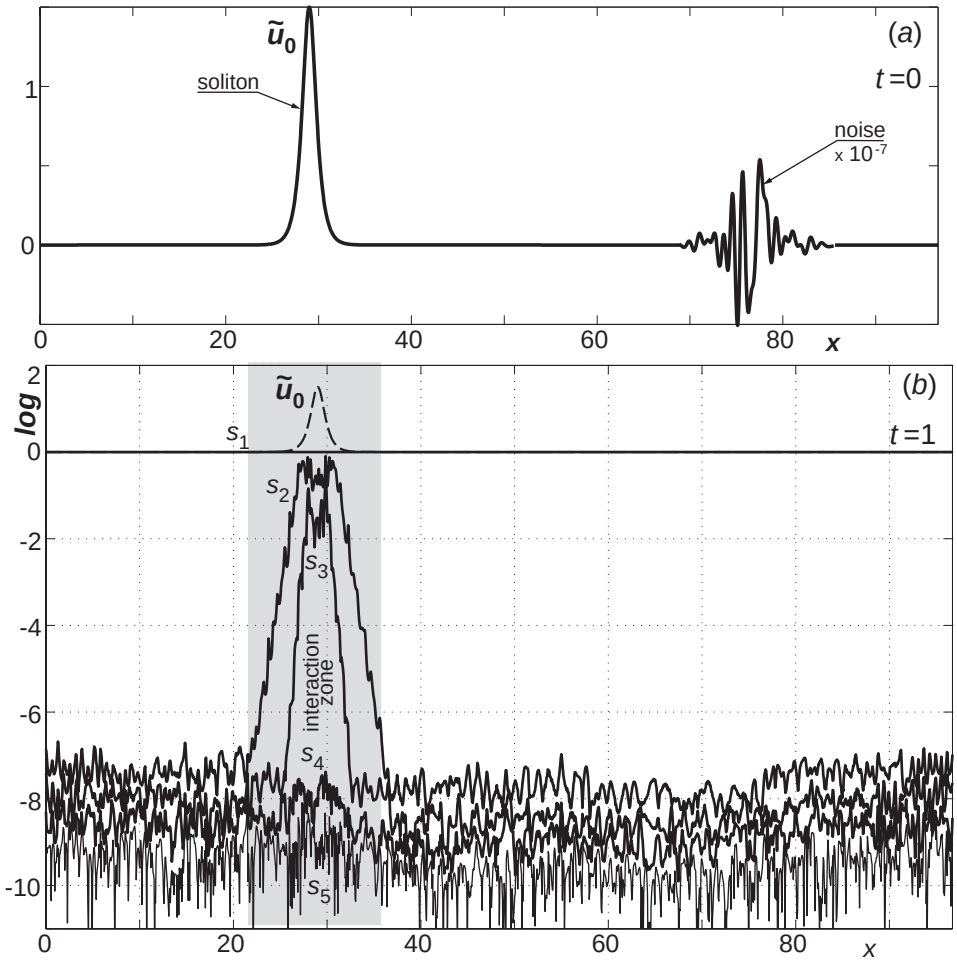

Figure 5. The local analysis, weak modulation of the MKdV bell-shape soliton: (*a*) The initial configuration (the noise is presented schematically). (*b*) The dependence of the singular numbers versus the coordinate (the solid lines) and the solution profile (the hatched line, schematically) at one of the moments of the interactions.

without loss of generality including the integration constant to θ. As a result, our SF takes the form

$$u(x,t) \simeq F\Big(k_{\rm s}x - k_{\rm s}^3 t, \theta, \theta_x, \theta_{xx}\Big), \tag{3.29}$$

where there are only three modulated parameters, that the experiments reveal. For equation (3.2) this means that the coefficient of the leading derivative becomes equal to zero, which leads to the degeneration of the last one.

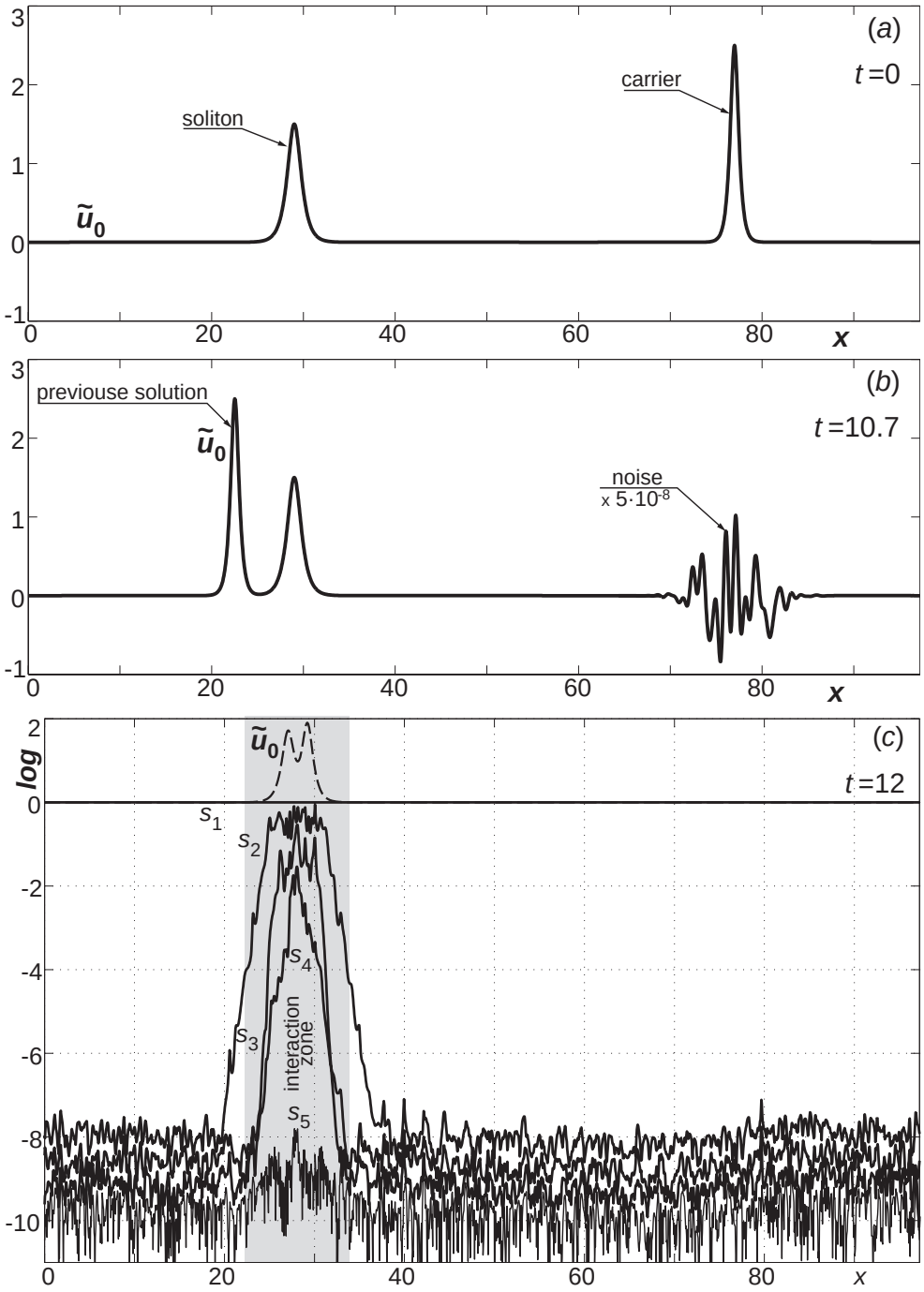

Figure 6. The local analysis, strong modulation of the MKdV bell-shape soliton: (a) The initial profile for $\tilde{u}_0$ in the first stage. (b) The initial profiles in the second stage with the schematically presented noise. (c) The dependence of the singular numbers versus the coordinate (the solid lines) and the solution profile (the hatched line, schematically) at the moment of the strongest carrier–soliton interaction.

4 The global analysis of dimensionality of IMSs and superposition formulae. The examples with the MKdV kink

4.1 The IMSs dimensionality

Consider now another experimental scheme addressed to the global analysis of IMSs.

For an equation of interest (2.1) take a series of the same kind of experiments with the initial conditions

$$u(x,0;\varphi) = u_{\text{soliton}}(x-\varphi,0) + u_{\text{perturbation}}(x), \qquad \varphi = \text{const} \tag{4.1}$$

differing only by the soliton position (the perturbation and soliton do not overlap each other) and with suitable boundary conditions (in particular in our examples these are periodic boundary conditions. If the superposition takes place, at any moment for these experiments we will have

$$u(x,t;\varphi) = F\Big(x-\varphi;\theta_1(x,t),\dots,\theta_n(x,t)\Big),$$

with $\theta_j(x,t)$ are the same for different φ, because in the framework of the MSP their evaluation does not dependent on the presence of the soliton, and the initial values are determined by the same perturbation. It is easy to see that in such manner, having $u(x,t;\varphi)$, we can restore the two dimensional function $u(x_1,x_2,t)$ itself. — After the change of the variables $\{x-\varphi = x_1, x = x_2\}$ one again has (2.6). Fixing here some moment of the interaction and the spacial coordinate, say t' and x', we will have a particular solution of the ODE (2.4)

$$u(x_1) = F\Big(x_1;c_1,\dots,c_n\Big), \qquad c_j = \theta_j(x',t'). \tag{4.2}$$

In principle, all such sample solutions can be chosen independently and arbitrarily, that can be used for determining the order of the last one. To be more precise, it is not hard to determine the order of any of its linearized versions and consequently its own order.

We now consider this matter separately. Assume that there is some set of samples $u_j(x_1)$ $(j=1,\dots,m; m>n)$ (4.2) close to each other and to another sample $u_0(x_1)$, i.e.

$$\begin{aligned} u_0(x_1) &= F\Big(x_1;c_{0,1},\dots,c_{0,n}\Big)\\ u_j(x_1) &= F\Big(x_1;c_{0,1}+\delta c_{j,1},\dots,c_{0,n}+\delta c_{j,n}\Big), \qquad |\delta| \ll 1, c_{j_1,j_2} = \text{const}. \end{aligned}$$

(Obviously, for the same t' and x' such samples can be obtained from close functions $u(x,t;\varphi)$. The last ones in their turn can be obtained as the solutions of the above initial-boundary value problems with close $u_{\text{perturbation}}(x)$.) Expending $u_j(x_1)$ into the Taylor series

$$\begin{aligned} u_j(x_1) = F|_{\vec{c}=\vec{c}_0} + \delta\Big(\frac{\partial F}{\partial c_1}\Big|_{\vec{c}=\vec{c}_0} c_{j,1} + \dots + \frac{\partial F}{\partial c_n}\Big|_{\vec{c}=\vec{c}_0} c_{j,n}\Big) + \mathrm{o}(\delta)\\ \vec{c} = (c_1,c_2,\dots,c_n), \vec{c}_0 = (c_{0,1},c_{0,2},\dots,c_{0,n}), \end{aligned}$$

one has for the differences $u_j - u_0$ in the leading order approximation

$$\Delta u_j(x_1) = u_j(x_1) - u_0(x_1) \approx \delta\Big(c_{j,1}\Psi_1(x_1) + \cdots + c_{j,n}\Psi_n(x_1)\Big), \tag{4.3}$$

where $\{\Psi_1, \ldots, \Psi_n\}$ are some set of linear independent functions. This means that in our approximation the maximum n of the differences Δu_j may be linearly independent

$$\max_{\text{all sets}} \dim\{\Delta u_1, \ldots, \Delta u_m\} = n.$$

In practice, since under a computer simulation we usually deal with mesh functions, and the $u_j(x_1)$ should tend to constants far from the soliton centre, the problem is reduced to the calculation of the rank of the matrix

$$\hat{A} = \begin{pmatrix} \Delta u_1(hi_1) & \Delta u_2(hi_1) & \ldots & \Delta u_m(hi_1) \\ \Delta u_1(hi_2) & \Delta u_2(hi_2) & \ldots & \Delta u_m(hi_2) \\ \ldots\ldots\ldots\ldots\ldots\ldots\ldots\ldots\ldots\ldots\ldots\ldots\ldots\ldots\ldots\ldots \\ \Delta u_1(hi_{m'}) & \Delta u_2(hi_{m'}) & \ldots & \Delta u_m(hi_{m'}) \end{pmatrix} \tag{4.4}$$

for a large enough number of mesh points m' and some step h, so that

$$\max_{\text{all sets}} \operatorname{rank} \hat{A} = n.$$

As before, instead of 'all sets', a large enough number of $\Delta u_j(x_1)$ associated with randomly generated functions $u_{\text{perturbation}}$ can be taken. Technically the procedure becomes especially simple in the case when $u_0(x_1)$ corresponds to an unperturbed soliton envelope, and Δu_j by this means correspond to its weak deformations. Similar experiments with weak modulation of a soliton by small perturbations is described in detail in Section 3.2.

Example 4 (determining a number of modulated parameters of the MKdV kink). Consider the above approach applied to the case with the kink (3.10) of the MKdV equation (3.7)

By virtue of the periodic boundary conditions the specific perturbation was again chosen in (4.1)

$$u(x,0) = u_{\text{kink}}(x-\varphi,0) + \Big[u_{\text{anti-kink}}(x-\varphi') + \delta u_{\text{localized noise}}(x-\varphi')\Big], \tag{4.5}$$
$$|\delta| \ll 1,\ \varphi, \varphi' = \text{const},\ \max|u_{\text{localized noise}}| = 1,$$

where φ and φ' set the initial positions of the kink and perturbation, and the function $u_{\text{localized noise}}(x)$ corresponds to some signal in the form of a noise localized near the point $x = 0$. In contrast to the last one, the anti-kink does not interact with the kink under investigation at all because it moves with the same velocity, but its presence allows one to satisfy the boundary conditions.

In order to obtain a sample $u_j(x_1)$ it is necessary to carry out a whole series of experiments with different φ in (4.1), (4.5). In view of this it is convenient to present all data and results for them at once, as two dimensional functions of x and φ. In Figure 7 the initial profiles (4.5) are depicted in such a manner. In the simulations $\varepsilon \sim 10^{-17}$ and $\delta = 10^{-8}$ respectively at $k_{\text{s}} = 2$. In the figure the component $u_{\text{localized noise}}$ is scaled

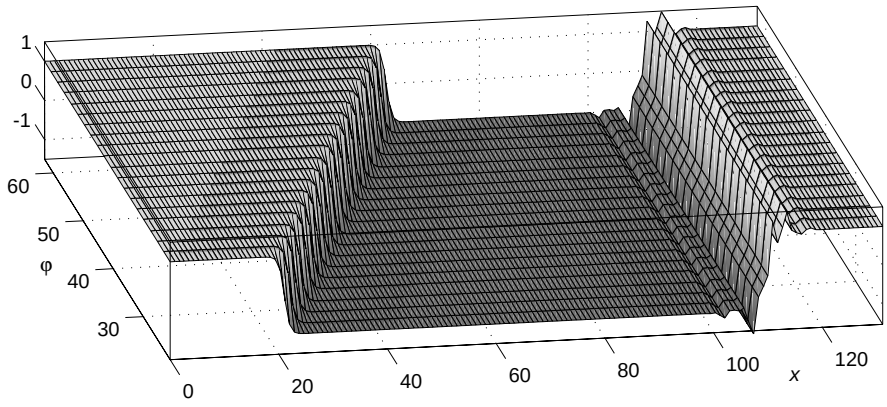

Figure 7. (The global analysis, the experiments with the MKdV kink). The two-dimensional function $u(x,0;\varphi)$ (4.5) corresponding to the initial data profiles (the component $u_{\text{localized noise}}$ was scaled for the visuality).

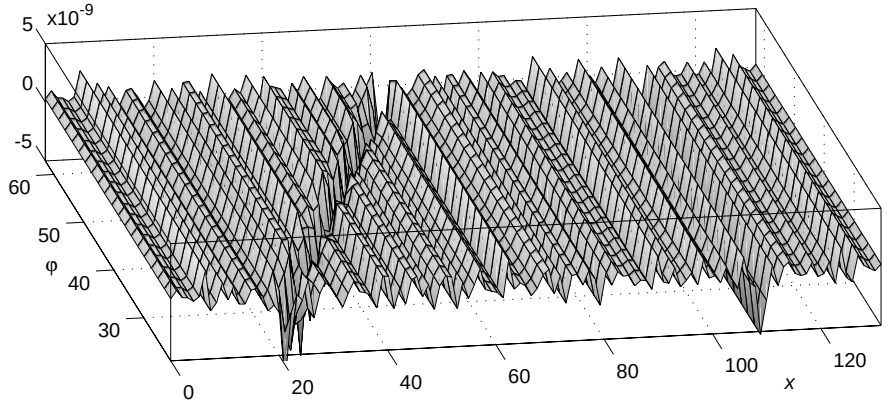

Figure 8. (The global analysis, the experiments with the MKdV kink). The two-dimensional function $\Delta u(x,t;\varphi)$ at $t=25$.

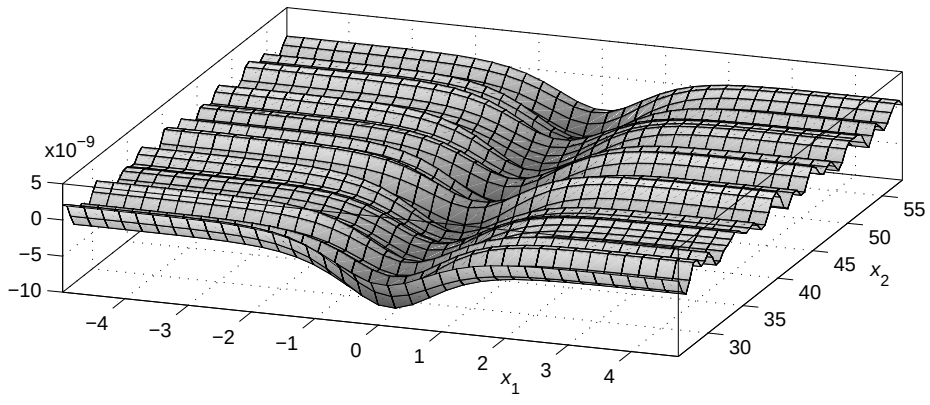

Figure 9. (The global analysis, the experiments with the MKdV kink). The picture of the profiles $\Delta u(x_1)$ versus x_2 obtained at $t'=25$ and $x'=x_2$.

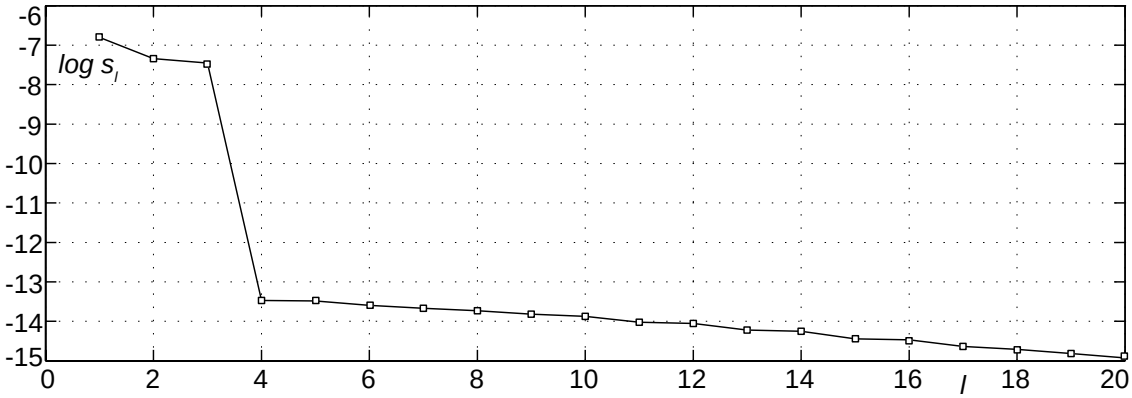

Figure 10. (The global analysis, the experiments with the MKdV kink). The diagram of the first singular numbers s_l of the matrix A constructed from the samples depicted in Figure 9.

by the factor $1/\delta$ for clarity of vision, i.e. in fact we see the image of the function $u_{\text{kink}} + u_{\text{anti-kink}} + u_{\text{localized noise}}$.

The next step is, of course, the use of a coordinate system in which a soliton is unmovable, which essentially simplifies further result processing. One more useful idea is to take as samples also sections corresponding to various x' and, if needed, t'. The former however is possible only when $u_0(x,t)$ corresponds to an unperturbed soliton solution, while the latter implies that Ψ_j in (4.3) does not depend on choosing t' (such an assumption seems to be natural for the usual static solitons taken in the above coordinate system, but it is obviously invalid, say, for breathers).

The next figure, Figure 8, demonstrates the profiles of the related differences $\Delta u(x,t) = u(x,t) - u_0(x,t)$ (here $u_0(x,t)$ is the solution with the undeformed kink corresponding to the initial data (4.5) with $u_{\text{localized noise}} = 0$) at one of the moments of interaction, when the initially localized perturbation has spread to all the space and modulated the kink. The sections $\Delta u(x_1)$ at the same moment of time versus the variable x_2 (instead of the index 'j' in (4.3) as proposed) are depicted in Figure 9.

Figure 10 shows the first twenty singular numbers obtained by processing the matrix $\hat{A}$ (4.4) with 120 samples on 37 points, $m = 120$ and $m' = 37$ in our notations. As the samples, the above sections for $t' = 25$ and x' ($x' = x_2$) uniformly distributed from 25.74 to 57.87 are generated from the only series of the initial data (Figure 7). As seen from the plot, three singular numbers sharply dominate, with the values of the remaining ones standing at the calculation error level, so that with high reliability one can conclude that the kink–perturbation interactions can be described by an SF with three modulated parameters, which is in agreement with SF (3.9). Moreover, the results mean that for small perturbations $u(x_1, x_2, t)$ should have the form

$$u(x_1, x_2, t) = \tanh(x_1 + 2t) + \delta \sum_{j=1}^{3} \theta_j(x_2, t)\Psi_j(x_1 + 2t) + \mathrm{o}(\delta), \tag{4.6}$$

although the linkages between $\theta_j(x_2, t)$, the equations governing their evolution, and the functions Ψ_j remain unknown yet.

4.2 Superposition formulae for a soliton and low amplitude waves

The natural question that arises now is: Whether it is possible also to restore a full expression for SFs similar to (4.6)?

Assume again that for a nonlinear PDE of interest (2.1) we deal with a static soliton moving with the speed $v_{\rm s}$, so that the SF sought takes the simplest form already indicated above

$$u(x_1,x_2,t)=u_{\rm soliton}(x_1-v_{\rm s}t)+\delta\sum_{j=1}^{n}\theta_j(x_2,t)\Psi_j(x_1-v_{\rm s}t)+{\rm o}(\delta),\quad v_{\rm s}={\rm const}. \tag{4.7}$$

Concerning the functions Ψ_j, the solution is trivial. Really, from the properties of SVD, we know that their mesh versions are identical to the columns of the matrix $\hat{U}$ in the SVD presentation (3.4) of $\hat{A}$ (4.4). More precisely, these are the first n of its columns associated with dominant singular numbers.

Next, substituting (4.7) into the adjoint equation (2.2) and omitting terms of the second and higher order in δ, one will have the linearization of (2.2) on the background of the solution $u_{\rm soliton}$, which turns into an identity under appropriately chosen relations for the functions θ_j. How to find these relations? The naive point of view is to fix some values of x_1, because the dependence on it is known, and to investigate the overdetermined PDEs systems to θ_j being obtained after this. This is not the best idea because, in particular, all available data are obviously corrupted by computational errors, and we do not even know what it means to find an approximately compatible system of PDEs from their overdetermined set. One more serious reason against this choice is that for our further purposes we want to work out an approach just for similar incompatible systems.

Let the functions θ_j be representable by the Fourier integrals

$$\theta_j(x_2,t)=\int\limits_{-\infty}^{+\infty}b_j(k){\rm e}^{(ikx_2+\omega(k)t)}{\rm d}k. \tag{4.8}$$

Then the above-mentioned linearized equation is converted into the relation

$$\int\limits_{-\infty}^{+\infty}\left\{\sum_{j=1}^{n}b_j(k)P_j\Big(k,\omega(k),[u_{\rm soliton}],[\Psi_j]\Big)\right\}{\rm e}^{(ikx_2+\omega(k)t)}{\rm d}k=0, \tag{4.9}$$

where P_j are some polynomials with respect to k with the coefficients depending on derivatives of $u_{\rm soliton}$ and Ψ_j. Instead of reducing of the left-hand side to zero, one will demand its minimization for every t according to the norm $\|\ \|_2$, i.e. the minimization of the following functional

$$J\left[\omega(k);b_1(k),\ldots,b_n(k)\right]=$$
$$\int\limits_{-\infty}^{+\infty}\int\limits_{-\infty}^{+\infty}\left|\int\limits_{-\infty}^{+\infty}\left\{\sum_{j=1}^{n}b_jP_j\Big(k,\omega,[u_{\rm soliton}],[\Psi_j]\Big)\right\}{\rm e}^{(ikx_2+\omega t)}{\rm d}k\right|^2{\rm d}x_1{\rm d}x_2.$$

After some transformations, changing the order of the integration and taking into account the orthogonality of the Fourier modes, the functional can be written down as

$$J\left[\omega(k); b_1(k), \ldots, b_n(k)\right] = \int\limits_{-\infty}^{+\infty} \widetilde{J}\left[b_1(k), \ldots, b_n(k)\right] \mathrm{e}^{2\mathrm{Re}\,\omega(k)t} \mathrm{d}k, \tag{4.10}$$

where $\widetilde{J}$ is another functional

$$\widetilde{J}\left[\omega(k); b_1(k), \ldots, b_n(k)\right] = \int\limits_{-\infty}^{+\infty} \left| \sum_{j=1}^{n} b_j P_j\Big(k, \omega, [u_{\mathrm{soliton}}], [\Psi_j]\Big) \right|^2 \mathrm{d}x_1. \tag{4.11}$$

In order that the last integral converges, it is necessary at least that its positively defined integrand tends to zero for $x_1 \to \infty$. Under the assumptions

$$\lim_{x_1 \to \infty} u_{\mathrm{soliton}}(x_1 - v_{\mathrm{s}}t), \lim_{x_1 \to \infty} \Psi_j(x_1 - v_{\mathrm{s}}t) = \mathrm{const}$$

this gives us

$$\lim_{x_1 \to \pm\infty} \sum_{j=1}^{n} b_j(k) P_j\Big(k, \omega(k), [u_{\mathrm{soliton}}], [\Psi_j]\Big) = Q(k, \omega) \sum_{j=1}^{n} b_j(k) \Psi_j(\pm\infty) = 0. \tag{4.12}$$

Where $Q(k, \omega)$ is a common coefficient at Ψ_j in P_j, which always exists simply because of the strength of the homogeneous structure of (4.7). The obvious requirement

$$Q(k, \omega) = 0 \tag{4.13}$$

determines the dispersion relation for the Fourier modes in (4.8).

Since both multipliers in the integrand of (4.11) are positive, and $\omega(k)$ is fixed by (4.13), one needs to minimize the functional $\widetilde{J}$ (4.11) in its turn (this is obviously identical to minimization of a Fourier-mode amplitude in (4.9)). The necessary condition for this is

$$\frac{\partial \widetilde{J}}{\partial b_{l_1}} = \sum_{l_2=1}^{n} b_{l_1}^* I_{l_2 l_1} = 0, \tag{4.14}$$

$$\frac{\partial \widetilde{J}}{\partial b_{l_1}^*} = \sum_{l_2=1}^{n} b_{l_1} I_{l_2 l_1} = 0, \qquad l_1 = 1, \ldots, n, \tag{4.15}$$

where

$$I_{l_2 l_1}(k) = I_{l_1 l_2}^*(k) = \int\limits_{-\infty}^{+\infty} P_{l_2} P_{l_1}^* \mathrm{d}x_1, \qquad l_1, l_2 = 1, \ldots, n. \tag{4.16}$$

The conditions (4.14) and (4.15) are obviously equivalent. The following properties of I and the coefficients b_j take place:

Proposition 2. If all data are correct, the matrix $\hat{I}$ (4.16) has to be singular in the related approximation.

Proof. The opposite would mean $b_j = 0$ for all j, which is impossible.

Note 2. As a rule, for IMSs we deal with a situation when all function–parameters θ_j in (2.6) can in one way or another be expressed through the only function (θ in our examples) that corresponds to a single degeneracy of $\hat{I}$. But more general types of superposition are possible in principle. The trivial example is obviously the superposition of n solutions in linear or nonlinear but linearizable equations. Consideration of such marginal cases, however, is beyond of the scope of the present work.

Proposition 3. (a) For evolution equations (2.1), and a single degenerated matrix $\hat{I}$, it is enough to seek the solutions for $b_j(k)$ in the class of polynomials of no more than order $2(n-1)N$, where N is the order of an equation (2.1) under investigation. (b) The solutions for $b_j(k)$ are not uniquely defined.
Proof. (a) For evolution equations an order of P_j in (4.9) with respect to k cannot be of higher order then N. Respectively, the maximal order of the elements in $\hat{I}$ (4.16) will be $2N$.

Since $\hat{I}$ is singular, we can choose one of the functions b_j being sought, say b_n for definiteness, as free and instead of (4.14) or (4.15) consider the following system

$$\begin{pmatrix} I_{11} & I_{12} & \dots & I_{1,n-1} \\ I_{21} & I_{22} & \dots & I_{2,n-1} \\ \dots & \dots & \dots & \dots \\ I_{n-1,1} & I_{n-1,2} & \dots & I_{n-1,n-1} \end{pmatrix} \begin{pmatrix} b_1 \\ b_2 \\ \dots \\ b_{n-1} \end{pmatrix} = -b_n \begin{pmatrix} I_{1,n} \\ I_{2,n} \\ \dots \\ I_{n-1,n} \end{pmatrix}. \tag{4.17}$$

In accordance with the Cramer rule one has for the remaining b_j

$$b_j(k) = \frac{b_n(k) \det \hat{\tilde{I}}_j(k)}{\det \hat{\tilde{I}}(k)}, \quad j = 1, \dots, n-1, \tag{4.18}$$

where $\hat{\tilde{I}}$ is the above truncated version of $\hat{I}$ in (4.17) with $\det \hat{\tilde{I}} \neq 0$, and $\hat{\tilde{I}}_j$ are its related modifications. Their determinants are the $2(n-1)N$ or less order polynomials on k. Choosing $b_n(k) = \det \hat{\tilde{I}}$, from (4.18) one will have the proposition being to be proved.

(b) This is the obvious consequence of the arbitrariness in choosing $b_n(k)$ above. For instance, we could also take $b_n(k) = p(k) \det \hat{\tilde{I}}$, when $p(k)$ is any polynomial.

Note 3. Proposition 3 can be easily generalized both to cases of other types of PDEs, and to cases with a matrix $\hat{I}$ of another degree of degeneracy. This, however, demands separate consideration of each case.

Proposition 4. For equation (2.1) with $u, x, t \in \mathbb{R}$ and real-value coefficients polynomials $b_j(k)$ have to possess the following property

$$b_j^*(k) = b_j(-k). \tag{4.19}$$

Proof. Since u, and as a consequence Ψ_j, are real, θ_j in their turn have also to be real. This implies that in (4.8)

$$\left(b_j(k) \mathrm{e}^{\omega(k)t}\right)^* = b_j(-k) \mathrm{e}^{\omega(-k)t},$$

or (4.19) after taking into account the structure of the dispersion relations.

All these propositions are important for the implementation of the technique being developed. The first of them gives a simple procedure for data verification and determining the band of perturbations wave-numbers where an SF sought is correct (see Section 5). The second allows us to reduce the problem of finding $b_j(k)$ to standard algebra, so that both symbolic computations systems and usual numerical packages can be effectively applied to this purpose. In doing so, we have to take into account the last proposition and consider (4.19) as the additional constraint reducing the exact problem to an approximate one. The matter is that, due to computational errors and a limited simulation accuracy, 'exact' solutions for b_j themselves appears to be approximate, so that relation (4.19) is violated. In our research we used the solutions of the systems to b_j analogous to (4.17) with this constraint in the least-square approximation sense, that is a natural approach for overdetermined or inconsistent system, because of errors in the systems.

In connection with all the aforesaid conditions, the most convenient approach to control the accuracy of SFs being obtained is to use the following estimate, which in principle depends on a wave number,

$$\varepsilon_{\text{residual}}(k) = \sqrt{\int_{-\infty}^{+\infty} \left| \sum_{j=1}^{n} b_j P_j \right|^2 \mathrm{d}x_1} \Bigg/ \sqrt{\int_{-\infty}^{+\infty} \left| \sum_{j=1}^{n} b_j \Psi_j \right|^2 \mathrm{d}x_1}$$

i.e. the ration between the $\| \ \|_2$ norms of a residual for each Fourier mode and its own $\| \ \|_2$ norm, see (4.8) and (4.9).

Finally, knowing $b_j(k)$ and a dispersion relation $Q(w,k)$, we can easily express θ_j in an SF like (4.7), in terms of the only function, say $\theta(x_2,t)$,

$$\theta_j(x_2,t) = b_j\left(-i\frac{\partial}{\partial x_2}\right)\theta(x_2,t) \tag{4.20}$$

satisfying a linear PDE

$$Q\left(\frac{\partial}{\partial t}, -i\frac{\partial}{\partial x_2}\right)\theta(x_2,t) = 0.$$

As a result, (4.7) takes the habitual form similar to, e.g., (3.9) or with the use of the scalar product

$$u(x_1,x_2,t) = u_{\text{soliton}}(x_1 - v_{\text{s}}t) + \delta\sum_{j=1}^{n}\left(\vec{a}_j, \vec{D}\theta(x_2,t)\right)\Psi_j(x_1 - v_{\text{s}}t) + \text{o}(\delta), \tag{4.21}$$

$$\vec{a}_j = (a_{j,0}, a_{j,1}, \ldots, a_{j,n_b}),\ \vec{D} = \left(1, \frac{\partial}{\partial x_2}, \frac{\partial^2}{\partial x_2^2}, \ldots, \frac{\partial^{n_b}}{\partial x_2^{n_b}}\right), v_{\text{s}} = \text{const},$$

$$n_b = \max_j \ \text{order}\, b_j(k),$$

where $\vec{a}_j$ is the vector of the real in view of (4.19) constants as defined by (4.20) associated with the coefficients in $b_j(k)$.

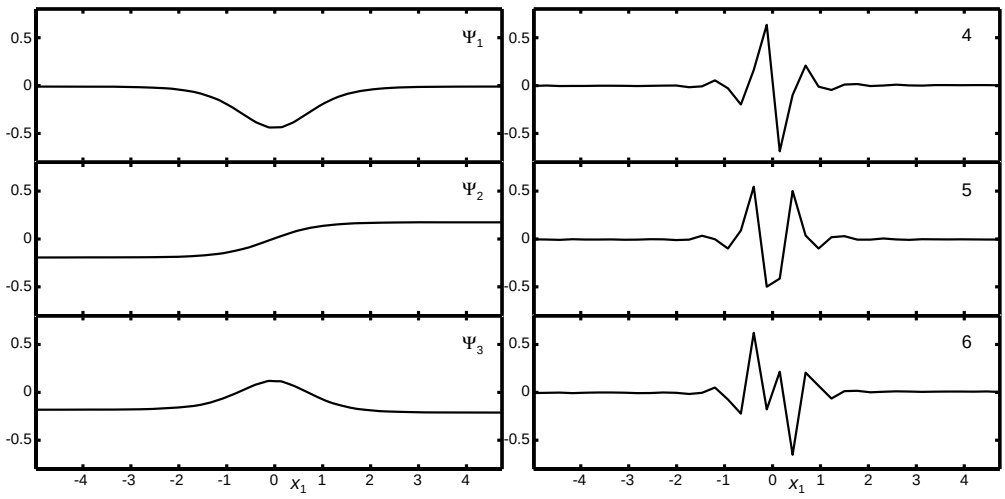

Figure 11. (The experiments with the MKdV kink, finding the SF). The profiles of first six basis functions in the SVD presentation of the matrix $\hat{A}$. First three of them are the true basis function $\Psi_j(x_1)$, the presence of the remaining ones are coursed by computational errors.

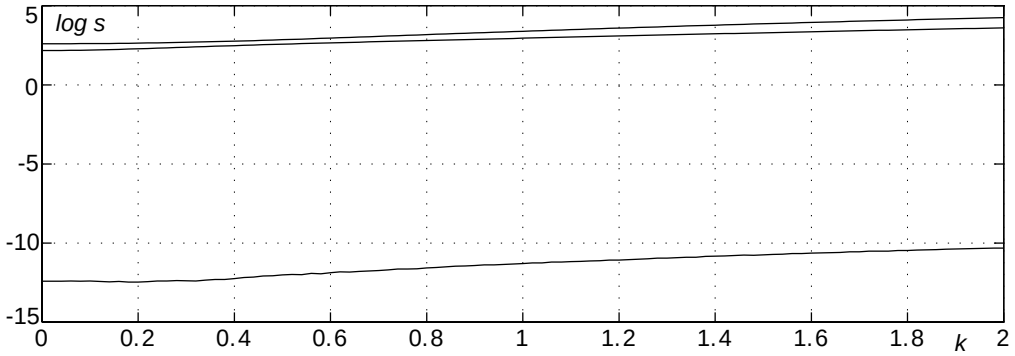

Figure 12. (The experiments with the MKdV kink, finding the SF). The dependencies of the singular numbers of the matrix $\hat{I}(k)$ on a wave number.

Example 5 (finding the SF for the MKdV kink). In Figure 11 the plots of the functions corresponding to the columns of the matrix $\hat{U}$ in the SVD (3.4) for $\hat{A}$ associated with the first six singular numbers from Figure 10 are depicted. Three of them are the functions Ψ_j in the SF sought, see (4.6), the remaining ones are caused by computational errors, and are of another character. The related expressions for P_j are as follows

$$P_j = \Psi_{j,x_1x_1x_1} + 3ik\Psi_{j,x_1x_1} + \left(\frac{k_\mathrm{s}^2}{2} - 6u_\mathrm{kink}^2 - 3k^2\right)\Psi_{j,x_1} + \left(\omega - 12u_\mathrm{kink}u_{\mathrm{kink},x_1} - 6iku_\mathrm{kink}^2 - ik^3\right)\Psi_j.$$

This immediately gives us, see (4.12), (4.13) and (3.10), the dispersion relation

$$\omega(k) = \frac{3}{2}ik_\mathrm{s}^2k + ik^3.$$

These expressions together with the above Ψ_j determine the matrix $\hat{I}(k)$ (4.16). As was indicating in Proposition 2, it has be singular, if our supposition about the existence of an SF and experiments are correct. Figure 12 shows the dependence of its singular numbers on k. As seen from this picture, $\hat{I}$ is really singular in our approximation at least for the band indicated.

Next, looking for $b_j(k)$, according to Proposition 3 we can restrict ourselves to consideration of the 12th order polynomials. However, a polynomial of second order provide the same accuracy. The final result for the SF is

$$
\begin{aligned}
&u(x_1,x_2,t)_{\text{experimental}} \approx \tanh(x_1+2t) \qquad (4.22)\\
&+\delta\Big[(-0.40841958860364\,\theta + 0.00255422119386\,\theta_{x_2} + 0.33125364905952\,\theta_{x_2x_2})\,\Psi_1\\
&+(0.00211348463161\,\theta + \theta_{x_2} + 0.03649662066592\,\theta_{x_2x_2})\,\Psi_2\\
&+(0.02170812942621\,\theta - 0.04955736892346\,\theta_{x_2} + 0.44975507103819\,\theta_{x_2x_2})\,\Psi_3\Big]\\
&\qquad \theta=\theta(x_2,t),\ \ \Psi_{1,2,3}=\Psi_{1,2,3}(x_1+2t)
\end{aligned}
$$

with $\varepsilon_{\text{residual}}|_{k=1} \approx 3.48\cdot 10^{-7}$, where θ is governed by the obvious PDE

$$\theta_t - \frac{3}{2}k_{\text{s}}^2\theta_{x_2} + \theta_{x_2x_2x_2} = 0, \qquad \theta=\theta(x_2,t)$$

By comparison, for the case of the weakly modulated parameters, the exact full SF (3.9) gives the following values in (4.21)

$$
\begin{aligned}
&\vec{a}_1 = (-0.408419598213, 0.00255424932619, 0.331253665152)\\
&\vec{a}_2 = (0.00211349465275, 1, 0.0364965945078)\\
&\vec{a}_3 = (0.0217081254769, -0.0495573527312, 0.449755076328)
\end{aligned}
$$

taking into account the decompositions on the segment $[0,L]$

$$
\begin{aligned}
1 &= -3.59959139139289\,\Psi_1 - 0.39659282666401\,\Psi_2 - 4.88729536091781\,\Psi_3\\
&\quad +r_1(x_1), \quad \|r_1\|_{2,\text{normalized}} \approx 3.41\cdot 10^{-7}\\
\tanh(x_1) &= 0.01387796551896\,\Psi_1 + 5.43328537925927\,\Psi_2 - 0.26925924002940\,\Psi_3\\
&\quad +r_2(x_1), \quad \|r_2\|_{2,\text{normalized}} \approx 2.05\cdot 10^{-7}\\
\tanh^2(x_1) &= -1.38053115981650\,\Psi_1 - 0.40807604625995\,\Psi_2 - 5.00524180168261\,\Psi_3\\
&\quad +r_3(x_1), \quad \|r_3\|_{2,\text{normalized}} \approx 3.56\cdot 10^{-7}\\
\|f(x)\|_{2,\text{normalized}} &= \sqrt{\frac{1}{L}\int\limits_0^L f^2(x)\mathrm{d}x}
\end{aligned}
$$

and the renormalization $\theta \to 0.368101408337\,\theta$ there. By this means the SF constructed (4.22) is in full agreement with the theory in the framework of the simulation accuracy.

Note that as a consequence of the structure of similar SFs for small amplitude perturbations we have a transparent enough mechanism of their transformation in the process

of an interaction. The coefficients in their Fourier expansions

$$u_{\text{perturbation}_{\text{before/after}}}(x_2,t)=u(\pm\infty,x_2,t)=\int\limits_{-\infty}^{+\infty}g_{\pm\infty}(k)\mathrm{e}^{[ikx_2+\omega(k)t]}\mathrm{d}k$$

before and after such an interaction are linked by *the transferring function*

$$\frac{g_{+\infty}(k)}{g_{-\infty}(k)}=T_{-\infty}^{+\infty}(k)=\frac{\sum\limits_j b_j(k)\Psi_j(+\infty)}{\sum\limits_j b_j(k)\Psi_j(-\infty)}.$$

In particular, for the above SF with the MKdV kink the last one has the form

$$T_{-\infty}^{+\infty}(k)=\mathrm{e}^{2\arctan\left(\frac{k_\mathrm{S}}{k}\right)i},$$

which is only the inhomogeneous phase shift.

5 Approximation by superposition formulae of a lower order. The Kawahara and RLW equations

For cases of infinitely dimensional IMSs or simply when the use of exact IMSs becomes impossible, the questions set out above take another form: Modulation of how many parameters in a soliton envelope have to be taken into account for the description of soliton–perturbation interactions to attain a certain accuracy? And in reality we already have an answer to it in hand.

Proposition 5. Let there to be some set of m_1 vectors $\vec{A}_j=(A_{1j},A_{2j},\dots,A_{m_2j})^{\mathrm{T}}$ with the SVD representation (3.4) of the matrix $\hat{A}_{ij}$, then their truncated expansions in terms of the basis $\{\vec{U}_1,\vec{U}_2,\dots,\vec{U}_m\}$

$$\vec{A}_{j,\text{approximate}}=\sum_{l=1}^{m'}s_lV_{jl}\vec{U}_l,\qquad m'<m$$

approximate the above systems of $\vec{A}_j$ as a whole with the following accuracy

$$\varepsilon_{\text{samples}}=\frac{\|A-A_{\text{approximate}}\|_F}{\|A\|_F}=\frac{\sqrt{\sum\limits_{i,j}\left(A_{ij}-A_{ij,\text{approximate}}\right)^2}}{\sqrt{\sum\limits_{i,j}A_{ij}^2}}=\frac{\sqrt{\sum\limits_{l=m'+1}^{m}s_l^2}}{\sqrt{\sum\limits_{l=1}^{m}s_l^2}}\qquad(5.1)$$

Proof. An SVD can be interpreted as an expansion of the vectors corresponding to the columns of a matrix under consideration in terms of the specific basis formed by the columns of the matrix $\hat{U}$

$$\vec{A}_j=\sum_{l=1}^{m}s_l\hat{V}_{jl}\vec{U}_l$$

This is specific, in the sense that the columns of the matrixes $\hat{U}$ and $\hat{V}$ are orthonormal (3.5). Taking into account the last situation, one directly has

$$\|A - A_{\text{approximate}}\|_F^2 = \sum_{i,j} \left(\sum_{l=m'+1}^{m} \hat{U}_{il} s_l \hat{V}_{jl} \right)^2 = \sum_{i,j} \left(\sum_{l_1=m'+1}^{m} \hat{U}_{il_1} s_{l_1} \hat{V}_{jl_1} \right)$$
$$\times \left(\sum_{l_2=m'+1}^{m} \hat{U}_{il_2} s_{l_2} \hat{V}_{jl_2} \right) = \sum_{l_1,l_2=m'+1}^{m} \left(\sum_i \hat{U}_{il_1} \hat{U}_{il_2} \right) \left(\sum_j \hat{V}_{jl_1} \hat{V}_{jl_2} \right) s_{l_1} s_{l_2}$$
$$= \sum_{l_1,l_2=m'+1}^{m} \delta_{l_1 l_2}^2 s_{l_1} s_{l_2} = \sum_{l_1=m'+1}^{m} s_{l_1}^2$$

and respectively (for instance, setting $m' = 0$)

$$\|A\|_F^2 = \sum_{l=1}^{m} s_l^2.$$

This gives (5.1).

Although $\varepsilon_{\text{samples}}$ is not identical to $\varepsilon_{\text{residual}}$ (see the next section), there is obviously a direct connection between them, and the sense of this proposition for us is very simple. We can construct an acceptable order SF if we sacrifice accuracy. Another aspect of this matter is that we can obtain an arbitrary accuracy remaining in the class of finite order SFs.

The following examples with the Kawahara and Regularized Long Waves equations demonstrate the aforesaid. Both equations are assigned to so-called nonintegrable nonlinear PDEs, and basically they are the generalizations of the usual KdV equation. An interested reader can find more about them, e.g., in [21, 12]. From more recent years we note here the research papers [10, 14, 17].

As a whole, the research scheme does not differ from the examples with the MKdV kink, and we will just present its results. Again, a coordinate system moving with the solitons was used in the simulation.

Example 6 (the Kawahara equation). In a number of works it was shown that the Kawahara equation

$$u_t + uu_x - u_{xxx} + u_{xxxxx} = 0, \qquad u = u(x,t) \tag{5.2}$$

has the exact soliton solution

$$u_{\text{soliton}}(x - \varphi, t) = -\frac{105}{169} \cosh^{-4} \left(\frac{x + \frac{36}{169} t - \varphi}{2\sqrt{13}} \right), \quad \varphi = \text{const}.$$

Figure 13 schematically, i.e. with scaling $u_{\text{localized noise}}$ by a factor $1/\delta$ at $\delta = 10^{-8}$ ($\varepsilon = 10^{-17}$), depicts the typical profiles for the initial data used in the experiments

$$u(x, 0; \varphi) = u_{\text{soliton}}(x - \varphi, 0) + \delta u_{\text{localized noise}}(x - \varphi'), \quad |\delta| \ll 1, \tag{5.3}$$
$$\varphi, \varphi' = \text{const}, \ \max |u_{\text{localized noise}}| = 1$$

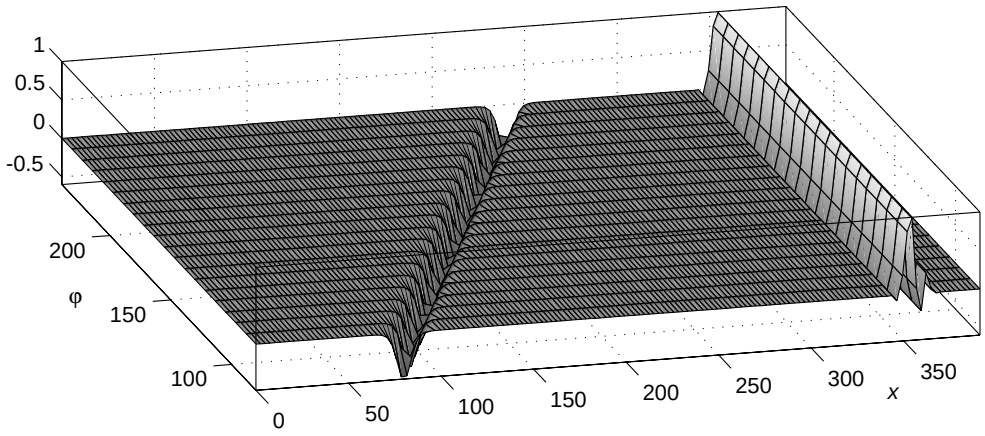

Figure 13. (The experiments with the Kawahara equation soliton). The two-dimensional function $u(x, 0; \varphi)$ (5.3) corresponding to the initial data profiles in one of the series of the experiments (the component $u_{\text{localized noise}}$ was scaled for the visuality).

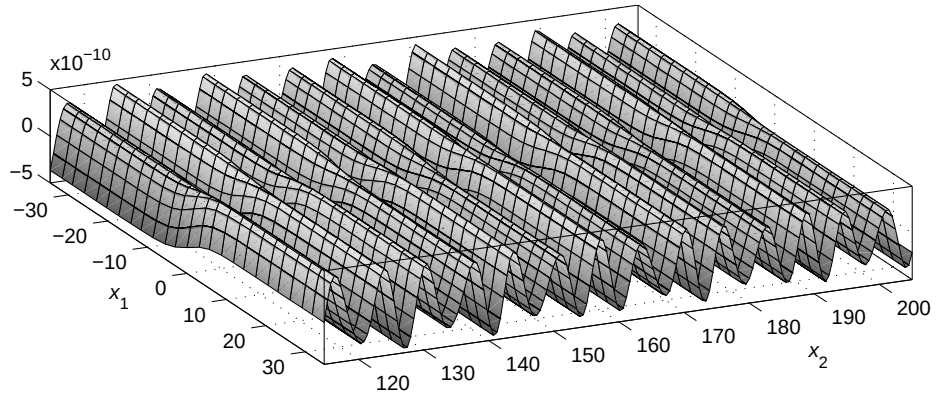

Figure 14. (The experiments with the Kawahara equation soliton). The picture of the profiles $\Delta u(x_1)$ versus x_2 obtained at $t' = 25$ and $x' = x_2$ from the initial data depicted in Figure 13.

while the form of the profiles for $\Delta u(x_1)$ arising in doing so is shown in Figure 14. In their turn Figures 15 and 16 show the diagram for the first singular numbers together with the related values of $\varepsilon_{\text{samples}}$ and the plots of several first basis functions $\Psi_j(x_1)$. The last ones are associated with the matrix $\hat{A}$ constructed from the data obtained in 7 series of experiments with various $u_{\text{localized noise}}$ for $t' = 25$ and x' uniformly distributed on the segment $[114.75, 205.02]$ with the step $h = 0.51$. In other words the matrix with 1246 samples on 137 points was processed. As seen from the diagram, six basis functions provide the accuracy with $\varepsilon_{\text{samples}}$ of the order 10^{-7}. The accuracy quickly increases with the number of basis functions being taken into account, up to the computational errors level.

The second part of the scheme gives the related coefficients in the SF sought in (4.7)

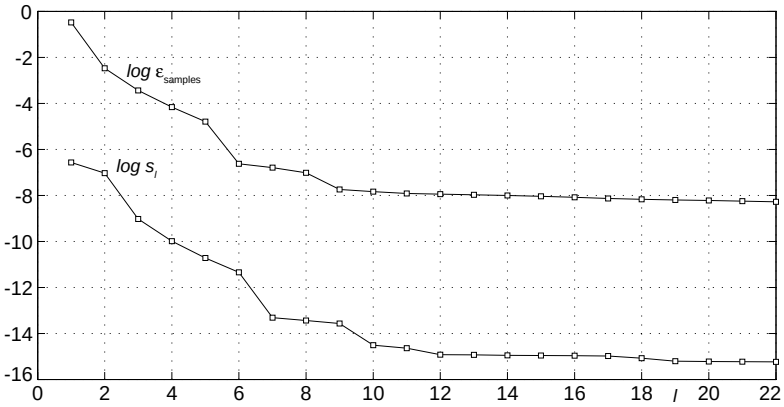

Figure 15. (The experiments with the Kawahara equation soliton). The diagrams of the first singular numbers of the matrix $\hat{A}$ and the related magnitudes $\varepsilon_{\text{samples}}$.

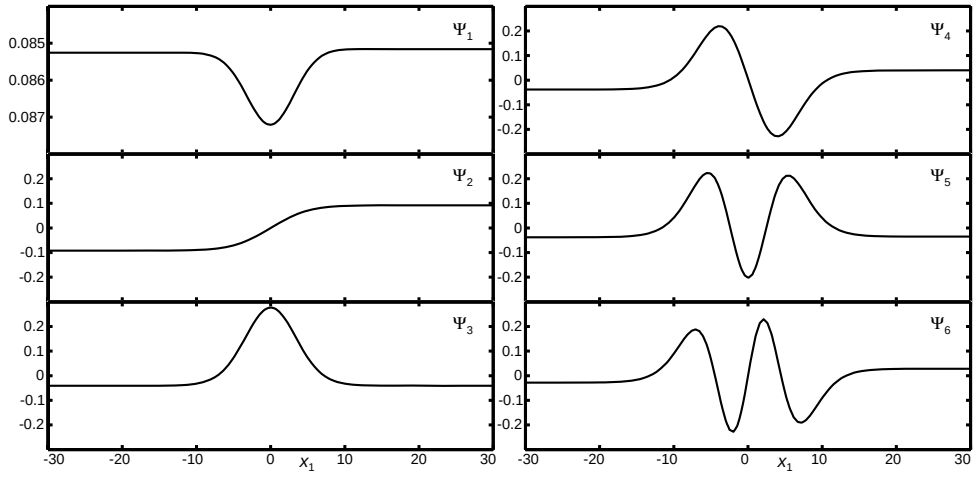

Figure 16. (The experiments with the Kawahara equation soliton). The profiles of first six basis functions $\Psi_j(x_1)$.

and (4.21). From the original equation (5.2) we have for P_j the following expression

$$P_j = \Psi_{j,x_1x_1x_1x_1x_1} + 5ik\Psi_{j,x_1x_1x_1x_1} - (10k^2+1)\Psi_{j,x_1x_1x_1} - ik(10k^2+3)\Psi_{j,x_1x_1}$$
$$+\left(u_{\text{soliton}} + 5k^4 + 3k^2 + \frac{36}{169}\right)\Psi_{j,x_1} + (u_{\text{soliton},x_1} + iku_{\text{soliton}} + ik^5 + ik^3 + \omega)\Psi_j$$

that in particular immediately gives

$$\omega = -ik^3 - ik^5$$

or respectively the evolution equation

$$\theta_t - \theta_{x_2x_2x_2} + \theta_{x_2x_2x_2x_2x_2} = 0, \qquad \theta = \theta(x_2, t)$$

Table 1. (The experiments with the Kawahara equation soliton). The values of the coefficients in (4.21) corresponding to the SF found with $n = 6$ and $n_b = 9$.

$\vec{a}_1$	$\vec{a}_2$	$\vec{a}_3$	$\vec{a}_4$	$\vec{a}_5$	$\vec{a}_6$
0.0000488795	0.0052437003	0.0000445108	0.0019740397	0.0000510678	-0.0006057694
0.0318686939	0.0003438036	0.0184599829	-0.0000567442	0.0031057781	-0.0000363413
0.0005167683	0.1865890381	0.0003756256	0.0077635624	0.0002294238	-0.0004684984
0.2031157406	0.0010473728	-0.0127553917	-0.0001072476	0.0044964892	-0.0000209475
0.0015777880	-0.3511531760	-0.0002008941	0.0024437336	0.0000492868	0.0007200868
-0.7702349915	-0.0014665747	-0.0220753107	-0.0000357058	0.0008269880	-0.0000049525
-0.0046379157	0.3363143160	0.0002976764	-0.0037542391	-0.0000841735	0.0005617704
1.0000000000	-0.0005510736	0.0068048253	0.0000416618	-0.0001086343	-0.0000074914
0.0034316121	-0.0000026442	0.0000213071	-0.0000833229	-0.0000037744	0.0000087976
-0.6026014259	0.0003305423	-0.0035732559	-0.0000273894	0.0003262403	-0.0000003251

for the function θ in (4.21). Next, for the SF with six basis functions Figure 17 shows the degree of singularity of the matrix $\hat{I}(k)$ or, more precisely, the dependence of its singular values on the wave number, and Table 1 gives the values $\vec{a}_j$ in (4.21), respectively, with $n = 6$ at $n_b = 9$ (further growth of n_b cannot be accompanied by increasing the accuracy). These coefficients were obtained by minimizing $||\varepsilon_{\text{residual}}||_2$ in the wave numbers band $[0.8, 1.5]$, i.e. in the band where the above analysis of $\hat{I}(k)$ predicts a suitable validity of the SF (notice that in the perturbations $k \in [0, 1.5]$ at least, see the comments). — The dependence $\varepsilon_{\text{residual}}(k)$ is plotted in Figure 18. Finally, Figure 19 demonstrates the transferring function $T_{-\infty}^{+\infty}(k)$ for the SF that is found.

Example 7 (the RLW equation). The soliton solution for the RLW equation

$$u_t + uu_x + u_{xxx} - u_{txx} = 0, \qquad u = u(x,t) \tag{5.4}$$

is well known and has the following form

$$u_{\text{soliton}}(x,t) = \frac{12k_{\text{s}}^2}{1-4k_{\text{s}}^2}\cosh^{-2}\left(k_{\text{s}}x + \frac{4k_{\text{s}}^2}{4k_{\text{s}}^2-1}t - \varphi\right), \qquad k_{\text{s}}, \varphi = \text{const}.$$

As well as in the previous case with the Kawahara equation, the initial data for the experiments with the soliton under $k_{\text{s}} = 0.4$ are given by the expression like (5.3), and the related typical profiles, here with scaling $u_{\text{localized noise}}$ by factor $5/\delta$ for $\delta = 10^{-8}$ at $\varepsilon = 10^{-17}$, are depicted in Figure 20. Figure 21 is analogous to Figure 14 and demonstrates $\Delta u(x_1)$ for the above initial data. Processing the matrix $\hat{A}$ (147 by 1652) constructed from the samples obtained in 7 series of the similar experiments and corresponding to $t' = 740,800$ and x' chosen on the segment $[84.87, 132.84]$ with the step $h = 0.41$ brings us to the basis functions needed for deriving the SF. Figure 22 shows the diagrams for the singular numbers and the related $\varepsilon_{\text{samples}}$, while the functions Ψ_j themselves for $j = 1, \ldots, 6$ are depicted in Figure 23. Again, the basis from six first Ψ-modes describes the totality of all of these samples with $\varepsilon_{\text{samples}}$ of order 10^{-5}.

Our next step is the determination of the coefficients in the SF (4.21) with the basis function that is found. Taking into account the form of the expressions for P_j

$$P_j = (1+v_{\text{s}})\Psi_{j,x_1x_1x_1} + (3ik + 2ikv_{\text{s}} - \omega)\Psi_{j,x_1x_1} + (u_{\text{soliton}} - 2ik\omega - k^2v_{\text{s}} - 3k^2$$
$$-v_{\text{s}})\Psi_{j,x_1} + (u_{\text{soliton},x_1} + iku_{\text{soliton}} - ik^3 + k^2\omega + \omega)\Psi_j, \quad v_{\text{s}} = \frac{4k_{\text{s}}^2}{1-4k_{\text{s}}^2}$$

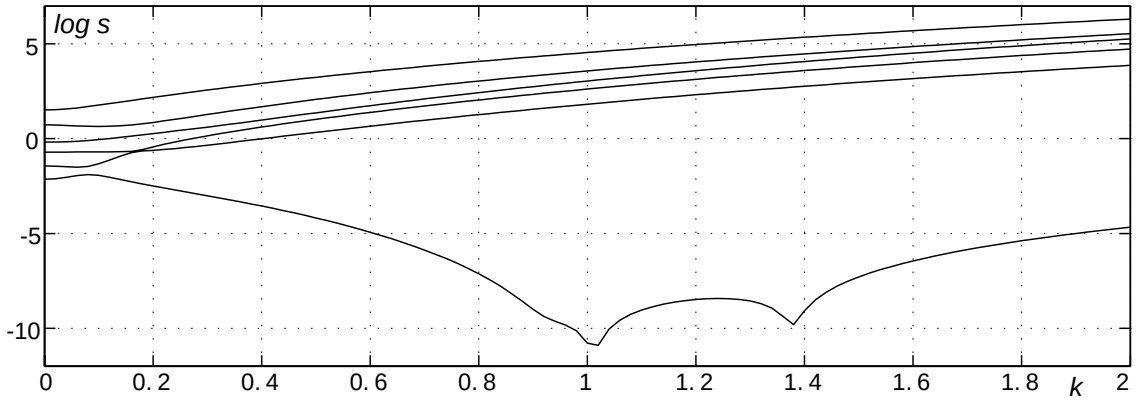

Figure 17. (The experiments with the Kawahara equation soliton). The singular numbers of the matrix $\hat{I}(k)$.

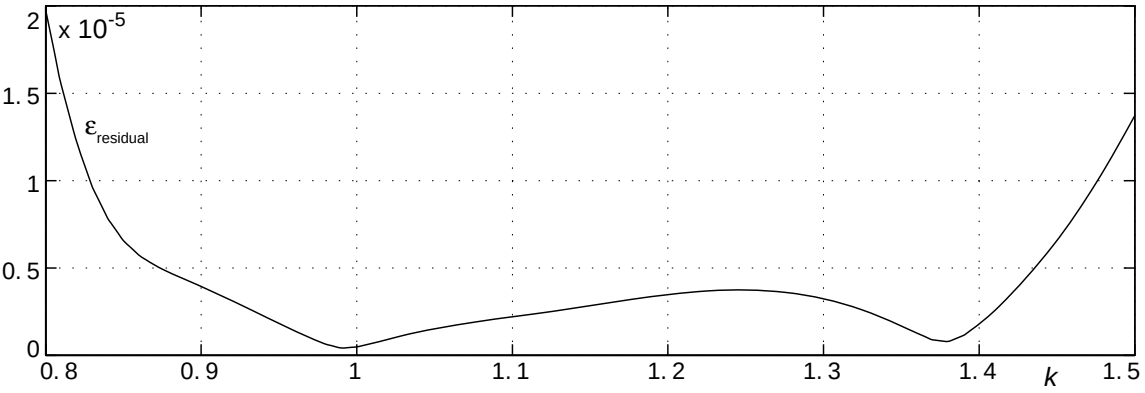

Figure 18. (The experiments with the Kawahara equation soliton). The plot of $\varepsilon_{\text{residual}}(k)$ reached for the SF with $n = 6$ and $n_b = 9$.

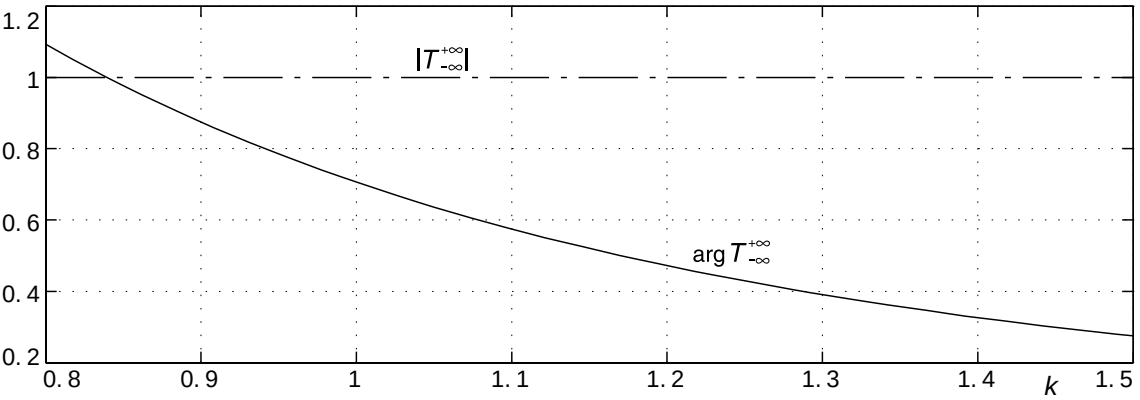

Figure 19. (The experiments with the Kawahara equation soliton). The module and argument of the transferring function $T_{-\infty}^{+\infty}(k)$ associated with the SF founded.

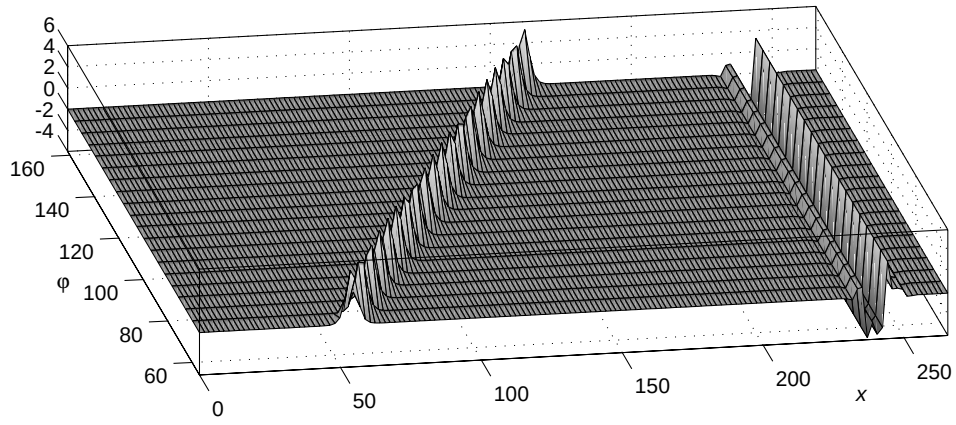

Figure 20. (The experiments with the RLW equation soliton). The two-dimensional function $u(x,0;\varphi)$ analogous to (5.3) corresponding to the initial data profiles in one of the series of the experiments (the component $u_{\text{localized noise}}$ was scaled for the visuality).

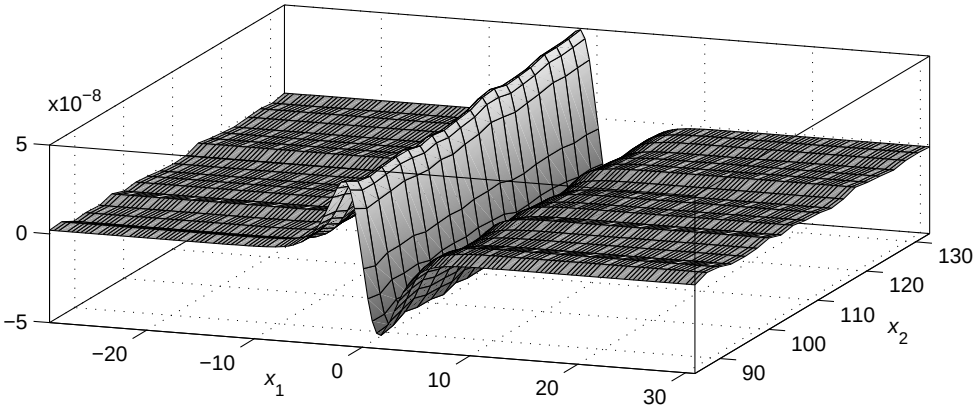

Figure 21. (The experiments with the RLW equation soliton). The picture of the profiles $\Delta u(x_1)$ versus x_2 obtained at $t' = 800$ and $x' = x_2$ from the initial data depicted in Figure 20.

one first of all has the dispersion relation

$$\omega = \frac{ik^3}{k^2+1}$$

and, as a result, the governing equation to the function θ

$$\theta_t + \theta_{x_2x_2x_2} - \theta_{tx_2x_2} = 0, \qquad \theta = \theta(x_2,t),$$

obviously representing just the linearization of the initial equation (5.4). As seen from Figures 24, the matrix $\hat{I}(k)$ for the SF with six basis function has a sufficient degree of singularity in the band $k \in [0, 1.1]$, that almost coincides with the range of wave numbers presented in the perturbations. The least-square minimization of $\varepsilon_{\text{residual}}(k)$ for this band leads to the values of $\vec{a}_j$ presented in Table 2 (again already $n_b = 9$ provides the maximal

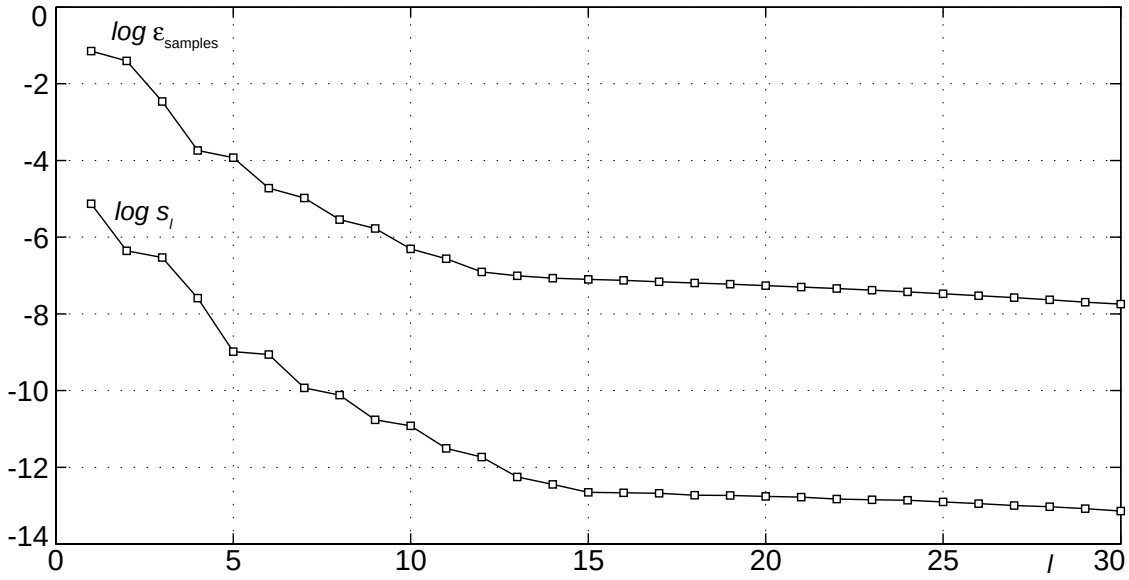

Figure 22. (The experiments with the RLW equation soliton). The diagrams of the first singular numbers of the matrix $\hat{A}$ the related magnitudes $\varepsilon_{\text{samples}}$.

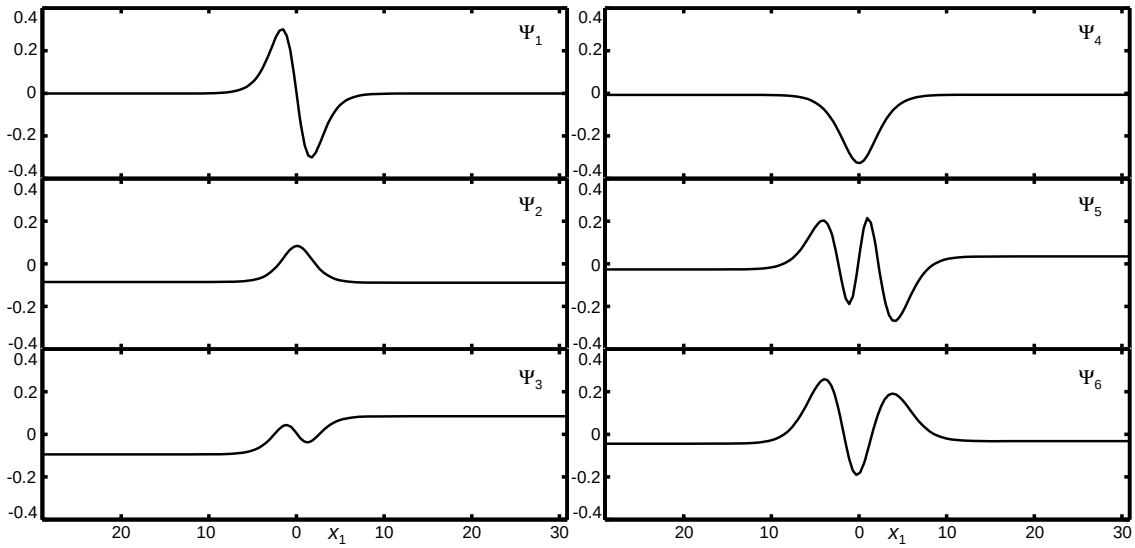

Figure 23. (The experiments with the RLW equation soliton). The profiles of first six basis functions $\Psi_j(x_1)$.

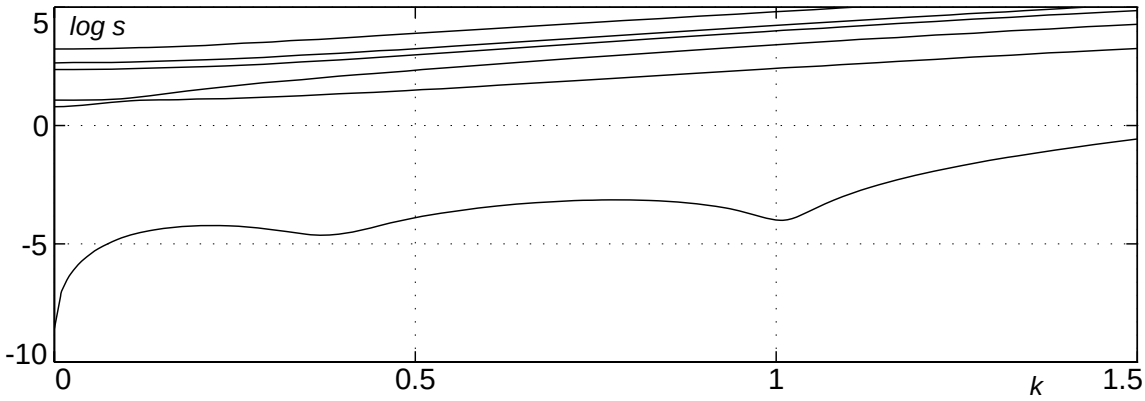

Figure 24. (The experiments with the RLW equation soliton). The singular numbers of the matrix $\hat{I}(k)$.

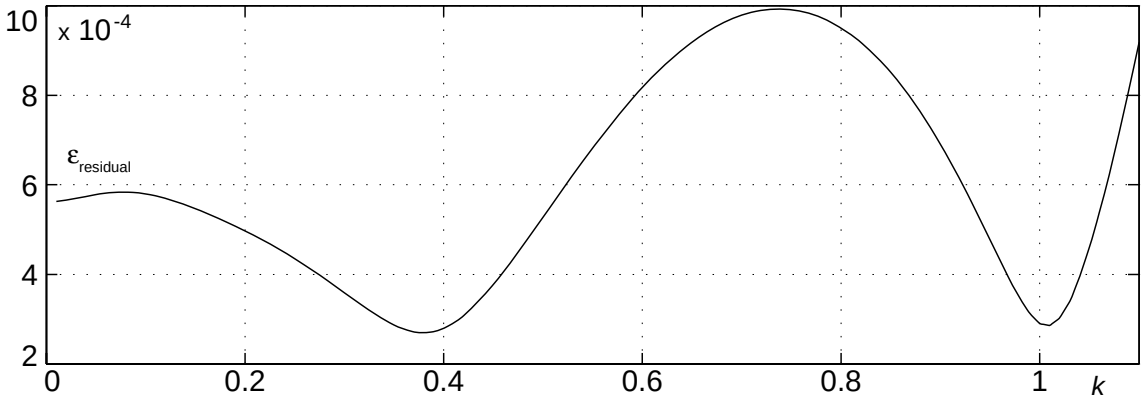

Figure 25. (The experiments with the RLW equation soliton). The plot of $\varepsilon_{\text{residual}}(k)$ reached for the SF with $n = 6$ and $n_b = 9$.

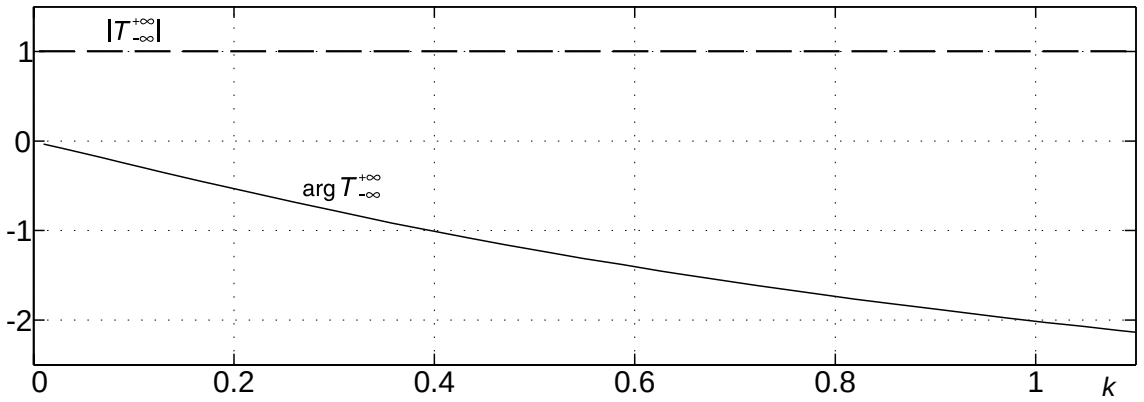

Figure 26. (The experiments with the RLW equation soliton). The module and argument of the transferring function $T_{-\infty}^{+\infty}(k)$ associated with the SF founded.

Table 2. (The experiments with the RLW equation soliton). The values of the coefficients in (4.21) corresponding to the SF found with $n = 6$ and $n_b = 9$.

$\vec{a}_1$	$\vec{a}_2$	$\vec{a}_3$	$\vec{a}_4$	$\vec{a}_5$	$\vec{a}_6$
0.0042876332	-0.0000478405	-0.0000033259	-0.0000017142	-0.0000010544	-0.0000001054
0.0003355579	0.0410447128	0.0007515110	0.0015011611	0.0000127152	-0.0000723397
-0.0453420679	-0.0036589309	0.0548630477	0.0000267593	-0.0005451342	-0.0000701499
-0.0013806016	-0.2472903276	-0.0060783973	-0.0018120629	0.0002044520	-0.0012434812
0.1907630693	0.0235406030	-0.3300824220	-0.0003578931	0.0015068325	0.0002112072
0.0040839882	0.7227282620	0.0238897827	-0.0225111123	-0.0004207060	0.0028466930
-0.3640683822	-0.0538102083	1.0000000000	0.0023505747	-0.0004591877	0.0000093219
-0.0011478866	-0.2417971986	-0.0103012815	0.1073398885	-0.0001926084	0.0004092835
0.1103363199	0.0193558992	-0.3969180587	-0.0008547960	-0.0061183991	-0.0009556559
-0.0008634079	-0.0824338115	-0.0013630094	-0.0374398554	0.0006651002	-0.0042288864

possible accuracy here). The magnitudes and distribution of $\varepsilon_{\text{residual}}(k)$ reached in doing so are plotted in Figure 25. Figure 26 shows the transferring function associated with the SF that has been constructed.

6 Some remarks and comments

Now all the results are available, and we can offer some comments and clear up some questions associated with the application of the technique that has been being developed.

First of all, it is not exaggerating if we underline the fact that although the idea to use computer simulation for deriving analytical expressions by itself is not very usual for the theory of PDEs, nevertheless all the methods applied are well known. Really, when performing a computer experiment to obtain the samples that are needed, we are in fact using Monte Carlo simulation, while the procedure for restoring SFs is close to that of the Kantorovich variational approach.

The results obtained in the experiments with the integrable equations (the finite dimensional IMSs) demonstrate practically ideal agreement, both quantitative and qualitative, with the theoretical data. Moreover, in the case with the MKdV bell-shape soliton they predict the degeneration of the SF that is confirmed by deeper analysis. In the global analysis the dimensionality of the IMSs and SFs are calculated directly, and this approach appears to be the most robust, while in the local analysis we can observe the dramatic growth of the related singular numbers in every point of the interaction zones (from the errors level 10^{-9}–10^{-7} up to the magnitudes 10^{-2}–1), that indicates to excitation of the same amount of the soliton envelope parameters. In doing so, the remaining singular numbers increase insufficiently by virtue of numerical effects.

There are several reasons for the enhancement of these remaining singular numbers. First, to balance a simulation accuracy and the contribution from the second order terms in (3.2) is practically impossible. Second, we cannot in principle digitalize a soliton envelope without involving roundoff errors. Moreover, as a consequence of the periodic boundary conditions, we in reality deal with some cnoidal waves close to a soliton under investigation in the domain under consideration, rather than the soliton itself. In particular, due to a similar distortion, noise there may appear as some excitation of singular numbers even far from a soliton, analogous to the effects on the soliton tail in Figures 4(*d*), 4(*e*). In addition

modulation may possess a cumulative effect and, with time, depending on a perturbation, the situation may become complicated. In particular, the initial assumption about the smallness of the perturbation influence may be violated.

Next, it is necessary to note separately that even in the simplest integrable cases, in order that all existing parameters should be excited in the appropriate measure, perturbations with a suitable spectrum are necessary. In the local analysis experiments we used noise with the wavenumbers $k \in [0, 7]$, that well provides such modulation.

In the cases with nonintegrable equations, where we have set another problem of approximation by a lower order IMSs, finding the correct basis functions is critical. There is no problem with this when exact SFs of a finite order are involved, but for infinite order SFs

$$u(x_1, x_2, t) = u_{\text{soliton}}(x_1 - v_{\text{s}}t) + \delta \sum_{j=1}^{\infty} \sum_{l=0}^{\infty} a_{j,l} \theta_{lx_2} \Psi_j(x_1 - v_{\text{s}}t) + \text{o}(\delta) \tag{6.1}$$

$$\theta = \theta(x_2, t), \ v_{\text{s}} = \text{const}$$

it is necessary to take into account the following circumstance: Depending on a perturbation spectrum, one or other of the basis functions will be dominant in (6.1). Strictly speaking, their set for, say, long wave perturbations, may appear to dramatically differ from an analogous set for short wave ones due to the difference in contributions from the low and high derivatives θ_{lx_2}. By this means the question on uniform approximation by lower order SFs or approximation in a given wave numbers band arises in such cases. In principle, in similar experiments we must chose perturbations with the spectrum adequate for further use of an SF being found in this way. These are demonstrated by examples with the Kawahara and RLW equations (see Figures 17, 18 and respectively 24, 25). Fortunately, it is not a very strong limitation for work with nonlinear PDEs that present real physical models, because of the original assumptions for their validity. Usually they are derived for certain circumstances, e.g., in the long wave limit, or for wave numbers around unity. In the case with the Kawahara equation it is necessary to pay attention to one more factor. The analysis of $\hat{I}(k)$ indicates that there is an issue with approximation in the band $k \in [0, 0.8]$, although these wave numbers are presented in the perturbations spectra. We can conclude from Table 1 (the first line, compare with Table 2 for the RLW equation) that most of the dependency on θ essential near zero remained in the basis functions unfound under this spectrum distribution. Perhaps the best solution in such cases would be the use of perturbations with narrow, delta function type spectra with a further combination of the resulting formulae.

We now offer some remarks about the sense of $\varepsilon_{\text{samples}}$ and $\varepsilon_{\text{residual}}$ being used in the estimations. In contrast to the latter, $\varepsilon_{\text{samples}}$ is a direct accuracy estimate. However, this is an accuracy just for a concrete set of samples. While $\varepsilon_{\text{residual}}$ is just a residual estimate, i.e. an indirect estimate of a solutions accuracy, but really reached for an SF with a given set of basis functions. For fully correct experiments, a real accuracy of an SF being sought has to tend to $\varepsilon_{\text{samples}}$ by probability. Here, notice that in our experiments we used more than mediocre statistics and the simplest technique in the Monte Carlo simulation. However, the approach justified itself quite clearly. Comparison of results based on the data obtained at various t', n, n_b, wave numbers bands and so on show that the dispersion is at least comparable with the accuracy being expected. For instance, for the transferring

functions, which accumulate in themselves all possible errors arising in each stage and step, the situation is as follows: Figure 19, the experiments with the Kawahara soliton, for $|T_{-\infty}^{+\infty}(k)|$ the dispersion and deviations from zero are about $3 \cdot 10^{-7}$ for the most part of the band rising up to about $2 \cdot 10^{-6}$ near its left boundary. For $\arg T_{-\infty}^{+\infty}(k)$ one has the dispersion of about 10^{-6} for the larger part and about $5 \cdot 10^{-6}$ near the left boundary. Analogously in the case of the RLW equation, Figure 26, the dispersion and deviations from zero are about $5 \cdot 10^{-5}$ for $|T_{-\infty}^{+\infty}(k)|$ with the exception of the left boundary, where they increase up to $2 \cdot 10^{-4}$. For $\arg T_{-\infty}^{+\infty}(k)$ one has $5 \cdot 10^{-4}$ and $2 \cdot 10^{-3}$ respectively. Here we explain that near to $k = 0$ the calculations with the polynomials used to obtain the coefficients in the SFs are sensitive to roundoff errors, and to obtain the best possible accuracy, the use of specialized software packages would be reasonable.

The cumulative effect may manifest itself in the global analysis as well. For instance, a phase shift is accumulated in passing perturbations through a soliton. As a result, with time, the contribution of the related Ψ-mode grows. The experiments with the RLW equation are a example of this. In Figure 21 the domination of the mode corresponding to the soliton phase is clearly defined. In the experiments with this equation a phase shift really dominates during soliton–perturbation interactions, in contrast to the experiments with the Kawahara equation soliton, where a phase shift is negligible in comparisons with the other types of deformation. The negative side of such accumulation and domination is that the related Ψ-modes, with time, force out other junior modes towards or beyond an error level excluding them from consideration, that in its turn leads to lost of an accuracy.

Finally, it is worth noticing that the perturbative nature of the methodology demands very high accuracy of a simulation in view of the relation $\varepsilon \sim \delta^2$. Say, to reach the accuracy of the data about 10^{-9}–10^{-7} in the experiments, we had to carry out the computations themselves with the accuracy $\varepsilon \sim 10^{-16}$ using all the capacity of 32-bit CPUs. In a number of cases, to realize a similar possibility, it is necessary additionally to take into account such specific numerical effects as aliasing errors and spectral blocking [28, 9] and to apply a special techniques to reduce their influence, e.g. via filtering or introducing so-called spectral viscosity [9, 8]. Also, at this accuracy level, the use of modern methods for stiff ODEs systems, e.g. [11], is essential from the viewpoint of time and stability of the calculations.

7 Conclusion

In this paper we develop the simplest techniques for an experimental investigation of invariant manifolds of the soliton type and for the partial restoring of the related superposition formulae, and demonstrate the *principle possibility of the similar approach* for researches of realistic models of mathematical physics (here we did not take as our purpose the obtaining of maximum accurate superposition formulae for further applications in various calculations). Both the integrable and nonintegrable systems, MKdV, KdV, Kawahara and RLW equations, are used as examples. Along with these examples, the future tasks for which a solution is necessary for effective implementation of the technique are indicated. More detailed study of these questions touched upon in the previous section is beyond the scope of this work because of its complexity, volume and mathematical speciality. We plan later to devote a separate paper to the above aspects, with special emphasis on the

theory for the above type of Monte Carlo simulation, because its effectiveness determines the accuracy of all further procedures.

Finally, it must be stressed that although here we have dealt only with SFs for solitons and low amplitude perturbations, such a class of problems is of no lesser interest for physical applications than strong soliton interactions. Among them are such problems as the propagation of optical pulses in real wave-guides, with various types of noise, pumping of nonlinear localized waves by linear waves, and the weak interactions of solitons, etc. One further field of application is the purely linear problems of diffraction and scattering in media with nonuniformities, e.g., in hydrodynamics and acoustics. Moreover, at the present moment, similar investigations are perhaps even more important from the viewpoint of engineering to take account the existing industrial technologies.

Acknowledgments. *The author is indebted to Professor A Jeffrey for his help. He is also grateful to Professor T Kawahara for encouragement and to Professor J P Boyd for the consultation and kindly given works [9, 8] as well as to Dr P C Matthews for his consultation. Finally, it would like to express the acknowledgment to Drs M Frigo and S G Johnson for their software package FFTW (http://www.fftw.org/) [18].*

References

[1] Agrawal G P, Nonlinear fiber optics, Academic Press, Inc., Boston, 1989.

[2] Alexeyev A A, Some notes on the singular manifold method: several manifolds and constraints, *J. Phys. A* **33** (2000), 1873–1894.

[3] Alexeyev A A, A multidimensional superposition principle: classical solitons I, *Phys. Lett. A* **278** (2001), 198–208.

[4] Alexeyev A A, A multidimensional superposition principle: classical solitons II, *J. Phys. A* **36** (2003), 9843–9864.

[5] Alexeyev A A, A multidimensional superposition principle and wave switching in integrable and nonintegrable soliton models, *J. Phys. A* **37** (2004), L627–L634.

[6] Alexeyev A A, A multidimensional superposition principle: classical solitons III, *Phys. Lett. A* **335** (2005), 197–206.

[7] Athorne C, Algebraic invariants and generalized Hirota derivatives, *Phys. Lett. A* **256** (1999), 20–24.

[8] Boyd J P, The Erfc-Log filter and the asymptotics of the Euler and Vandeven sequence accelerations, in *Proceedings of the Third International Conference on Spectral and High Order Methods*, *Houston J. Math.* (1996), 267–276.

[9] Boyd J P, Chebyshev and Fourier Spectral Methods, Dover Publications, Inc., New York, 2000.

[10] Bridges T J and Derks G, Linear instability of solitary wave solutions of the Kawahara equation and its generalizations, *SIAM J. Math. Anal.* **33** (2002), 1356–1378.

[11] Cox S M and Matthews P C, Exponential time differencing for stiff systems, *J. Comp. Phys.* **176** (2002), 430-455.

[12] Dodd R K, Eilbeck J C, Gibbon J D and Morris H C, Solitons and Nonlinear Waves Equations, Academic Press, London, 1982.

[13] Dodd R K, Equivalent Hirota bilinearisations, *Phys. Lett. A* **241** (1998), 257–261.

[14] Dye J M and Parkera A, An inverse scattering scheme for the regularized long-wave equation, *J. Math. Phys.* **41** (2000), 2889–2904.

[15] El'sgol'ts L E, Differential equations and calculus of variations, Nauka, Moscow, 1969 [Russian].

[16] Estévez P G *et al*, Modified singular manifold expansion: application to the Boussinesq and Mikhailov–Shabat systems, *J. Phys. A* **26** (1993), 1915–1925.

[17] Francius M, Pelinovsky E and Slunyaev A, Wave dynamics in nonlinear media with two dispersionless limits for long and short waves, *Phys. Lett. A* **280** (2001), 53–57.

[18] Frigo M and Johnson S G, The design and implementation of `FFTW3`, *Proceedings of the IEEE* **93** (2005), 216-231.

[19] Gibbon J D *et al*, The Painlevé property and Hirota's method, *Stud. Appl. Math* **72** (1985), 39–63.

[20] Kaptsov O V, Invariant sets of evolution equations, *Nonlinear Anal.* **19** (1992), 753–761.

[21] Kawahara T, Oscillatory solitary waves in despersive media, *J. Phys. Soc. Japan* **33** (1972), 260–264.

[22] Makhankov V G, Dynamics of classical solitons (in non-integrable systems), *Phys. Rep.* **35** (1978), 1–128.

[23] Musette M and Conte R, The two-singular-manifold method: I. Modified Korteweg-de Vries and sine-Gordon equations, *J. Phys. A* **27** (1994), 3895–3913.

[24] Gorshkov K A *et al*, Perturbation theory for kinks and its application for multisoliton interactions in hydrodynamics, *Phys. Rev. E* **69** (2004), 016614.

[25] Jakubowski M H, Steiglitz K, Squier R, Computing with solitons: A review and prospectus, *Mult.-Valued Log.* **6** (2001), 439–462.

[26] Parker A, On soliton solutions of the Kaup-Kupershmidt equation. I. Direct bilinearisation and solitary wave, *Physica D* **137** (2000), 25–33.

[27] Parker A, On soliton solutions of the Kaup-Kupershmidt equation. II. Anomalous N-soliton solutions, *Physica D* **137** (2000), 34–48.

[28] Press W H *et al*, Numerical Recipes in C, Cambridge University Press, Cambridge, 1992.

[29] Rodrigo M, Elmer C and Miura R M, A construction technique for heteroclinic solutions to continuous and differential–difference damped wave equations, *CAMS Report 0203-24* (2003).

[30] Schnitzer H J, Mertens F G and Bishop A R, A collective-variable theory for nonlinear coherent excitations in classical Hamiltonian systems, *Physica D* **141** (2000), 261–280.

[31] Scott A, Nonlinear science: emergence and dynamics of coherent structure, Oxford Unipersity Press, Oxford, 1999.